Investigating the role of FARP1 and RND3 in spatiotemporal regulation of signalling dynamics during collective cell migration

Katerina Zouboulakis
Department of Biology, McGill University, Montreal

July 2020

A thesis submitted to McGill University in partial fulfillment of the requirements of the degree of Master of Science (Biology)

Abstract

Collective cell migration is the migration of a group of cells that are interconnected through cell-cell junctions. Cells migrate autonomously, but are able to organize themselves and coordinate their motility through these connections. Migration is a polarized process that entails Rho (Ras homologous) GTPases to be organized along a front-to-rear axis and these components must be spatially and temporally regulated. Rho GTPases control cellular processes such as actin reorganization, motility, adhesion, and polarity through interactions with effector proteins. What is unclear is how Rho GTPase signalling is regulated in space and time during autonomous cell migration, and how this signalling is coordinated between neighbouring collectively migrating cells, across adhesive cell-cell contacts. A previously performed siRNA screen identified the Rho GEF FARP1, and the atypical Rho GTPase RND3, as candidate regulators of autonomous, and collective endothelial cell migration, respectively. Here, we investigate the molecular mechanisms by which FARP1 and RND3 regulate collective cell migration of human umbilical vein endothelial cells (HUVEC). We started by validating the results obtained from this screen using siRNA pool deconvolution and then determined knockdown efficiency using RT-qPCR. We then selected one siRNA from the pool and created an siRNA-resistant rescue construct to determine knockdown specificity. Lastly, using immunofluorescence, we observed and quantified changes in the actin cytoskeleton and myosin activity with RND3 knocked down or overexpressed. This work outlines the multiple steps taken to ensure that the results obtained by siRNA-mediated knockdown of Rho GEFs and Rho GTPases were not due to off-target effects, and provides further insight into the mechanisms by which collective cell migration is regulated.

Résumé

La migration cellulaire collective c'est la migration d'un groupe de cellules connectées par des jonctions intercellulaires. Les cellules se déplacent de manière autonome, mais sont capables de s'organiser et de coordonner leur motilité grâce à ces connections. La migration est un processus polarisée qui nécessite l'organisation des GTPases Rho le long de l'axe longitudinal de la cellule, ainsi que leur régulation spatiale et temporelle. En interagissant avec des protéines effectrices, les GTPases Rho contrôlent des processus tels que la réorganisation de l'actine, la motilité, l'adhésion, et la polarité cellulaire. La manière dont la signalisation des GTPases Rho est régulée dans l'espace et dans le temps durant la migration autonome, et comment cette signalisation est coordonnée entre cellules voisines lors du déplacement collectif, à travers les jonctions cellules-cellules, reste encore mal comprise. Un crible d'ARNsi (petit ARN interférent) déjà réalisé a permis d'identifier la GEF (facteurs d'échange de guanines) FARP1, et la GTPase Rho atypique RND3, comme candidats pour la régulation de la migration endothéliale autonome et collective, respectivement. Mon but est d'identifier les mécanismes par lesquels FARP1 et RND3 contrôlent la migration cellulaire collective en utilisant des HUVEC (cellules endothéliales humaines de la veine ombilicale). Nous avons commencé par valider les résultats obtenus grâce à la déconvolution du pool d'ARNsi, puis nous avons déterminé l'efficacité de la déplétion (knock-down) par RT-qPCR. Nous avons sélectionné un seul ARNsi du pool et nous avons créé une construction résistante a cet ARNsi afin de confirmer la spécificité du knock-down. Pour finir, grâce à des marquages immunofluorescents, nous avons visualisé et quantifié les changements de l'actine et de la myosine lorsque RND3 est déplété ou surexprimé. Ces données démontrent les plusieurs étapes prises afin d'assurer que les résultats obtenus par le crible d'ARNsi ciblant les GEFs et les GTPases Rho n'étaient pas dus à des effets «off-target», et permettent de mieux comprendre les mécanismes dont la migration collective est régulée.

Preface: Contributions of Authors

All experiments were performed and planned by myself under the guidance of Dr. Arnold Hayer. Additionally, he had performed the siRNA screening data (Figure 13), created the schematic demonstrating how coordination was calculated (Figure 14), and wrote the script used for determining Rho GEF and Rho GTPase expression analysis. All tables, data collection and analyses, and figures in the results section were prepared by myself. Dr. Minhee Kim helped me with the optimization of the RT-qPCR protocol, as well as with the calculations and data interpretation involved with this. This thesis was written by myself and revised and edited by Dr. Hayer. Dr. Muriel Sébastien helped with the correction of the French translation of the abstract.

Acknowledgments

I would first like to express my very great appreciation to my supervisor, Dr. Arnold Hayer, for letting me be a part of his lab as his very first graduate student. Thank you for guiding me through experiments, teaching me all the techniques I now know, and remaining positive, patient, and reassuring when things would not work out. I will forever be grateful for such a wonderful experience and opportunity. I would also like to thank my supervisory committee members, Dr. Claire Brown and Dr. Laura Nilson for their support, constructive criticism, and insightful suggestions over the last two years.

Many thanks to my Bellini second floor friends for the laughs and TC room gatherings and who were always willing to go out of their way to help me.

To my parents, grandparents, and sister Tina, you have consistently encouraged, listened, and supported me every step of the way. Most importantly, you believed in me even when I did not believe in myself, and helped me stay focused during challenging times. For this, I cannot thank you all enough. To Petro, you always help me regain perspective when I sometimes lose it. Your focus on the truly important and meaningful things in life is admirable and inspiring, and is something I strive to be mindful of every day. No matter what, you have never failed to be there for me and for that I am extremely thankful.

Table of Contents

List of Figures

List of Tables

List of Abbreviations

ADF	Actin-depolymerizing factor
Arp2/3	Actin-related protein-2/3
aPKC	Atypical protein kinase C
CAAX	C: Cysteine, A: Aliphatic amino acid, X: any amino acid
CR	Conserved region
DH	Dbl homology
DHR1	DOCK Homology Region 1
DHR2	DOCK Homology Region 2
DOCK	Dedicator of Cytokinesis
ERM	Ezrin-radixin-moesin
FAK	Focal adhesion kinase
FARP1	FERM, Rho GEF, pleckstrin homology domain protein
FAT	Focal adhesion targeting
FERM	4.1, ezrin, radixin, moesin
GAPDH	Glyceraldehyde-3-phosphate dehydrogenase
GAPs	Rho GTPase-activating proteins
GEFs	Rho guanine nucleotide exchange factors
GDIs	Rho guanine nucleotide dissociation inhibitors
GTP	Guanosine triphosphate
GDP	Guanosine diphosphate
HIVE-CUT	High-performance integrated virtual environment-codon usage tables
HUVEC	Human umbilical vein endothelial cells

LIMK	LIM kinase
mDia	Mammalian Diaphanous
MAP4K4	Mitogen-activated kinase kinase kinase kinase 4
MLC	Myosin light chain
MLCK	Myosin light chain kinase
MTOC	Microtubule organizing center
Rho	Ras homologous
RND3	Rho family GTPase 3
ROCK	Rho kinase
P-loop	Phosphate-binding loop
PAK	p21 activating kinase
PECAM-1	Platelet endothelial cell adhesion molecule-1
PH	Pleckstrin homology
PIP_2	Phosphatidylinositol 4,5-bisphosphate
PIP_3	Phosphatidylinositol 3,4,5-trisphosphate
PI3K	Phosphoinositide 3-kinase
PKC	Protein kinase C
pMLC	Phospho-myosin light chain
PTMs	Posttranslational modifications
siKIF11	Kinesin family member 11 siRNA
siNT	Non-targeting siRNA
siRNA	Small interfering RNA
Src	Proto-oncogene tyrosine-protein kinase Src

TPM	Transcripts per million
VASP	Vasodilator-stimulated phosphoprotein
VE-cadherin	Vascular endothelial cadherin
VEGF	Vascular endothelial growth factor
VE-PTP	Vascular endothelial protein tyrosine phosphatase
WASP	Wiskott-Aldrich syndrome protein
WAVE	WASP-family verprolin-homologous protein

1. INTRODUCTION

1.1 An overview of collective cell migration

Collective cell migration is characterized by the migration of cell groups, where individual cells are physically bound together by intercellular junctions (Scarpa and Mayor, 2016). These connections affect their behaviour and allows them to coordinate and cooperate (Scarpa and Mayor, 2016). Migration is more efficient when cells move collectively rather than individually (Mayor and Etienne-Manneville, 2016). There are many advantages to cells migrating collectively. Migrating cells can ensure that stationary cells, or cells moving in a different direction than the collective, follow the rest, and helps maintain correct tissue shape and structure during remodelling events (Mayor and Etienne-Manneville, 2016; Rørth, 2009). During tissue formation, interactions between collectively migrating cells also establishes correct cellular distributions (Rørth, 2009).

Collective cell migration is both essential and detrimental to our health (Horwitz and Webb, 2003). It maintains tissue homeostasis by regulating biological processes such as embryonic development and morphogenesis, and wound healing through the reparation of damaged tissue (Horwitz and Webb, 2003; Huttenlocher et al., 1995; Ridley et al., 2003; Rørth, 2009; Scarpa and Mayor, 2016). Collective cell migration also contributes to pathological processes including tumour metastasis, inflammatory diseases such as rheumatoid arthritis, and vascular diseases such as atherosclerosis (Horwitz and Webb, 2003; Huttenlocher et al., 1995; Mayor and Etienne-Manneville, 2016; Ridley et al., 2003; Scarpa and Mayor, 2016). Migration is a polarized process requiring Rho (Ras homologous) GTPases to be organized along a front-to-rear axis, and they must be spatially and temporally regulated (Cook et al., 2014; Llense and Etienne-Manneville, 2015).

1.2 Rho GTPases

1.2.1 Regulation of Rho GTPases

The 20 human members of Rho GTPases, grouped into 8 subfamilies, are part of the Ras superfamily of small GTPases (**Figure 1**) that control various cellular processes such as cell motility, adhesion, actomyosin rearrangement, polarity, and growth through interactions with effector proteins (Aspenström et al., 2007; Van Buul et al., 2014; Cook et al., 2014; Schaefer et al., 2014).

Rho GTPases are molecular switches that are regulated by Rho guanine nucleotide exchange factors (GEFs), Rho GTPase-activating proteins (GAPs) and Rho guanine nucleotide dissociation inhibitors (GDIs), (**Figure 2**), (Van Buul et al., 2014; Cook et al., 2014; Hanna and El-Sibai, 2013; Schaefer et al., 2014). Rho GEFs activate Rho GTPases by exchanging GDP for GTP, and Rho GAPs inactivate Rho GTPases by stimulating their hydrolytic activity so that GTP is hydrolyzed to GDP (Van Buul et al., 2014; Cook et al., 2014; Hanna and El-Sibai, 2013; Schaefer et al., 2014). Rho GTPases that cycle between these active and inactive forms are referred to as classical Rho GTPases (Aspenström, 2018). The binding of GTP induces a conformational change in Rho GTPases. This conformational change favours binding to downstream effector proteins, such as kinases and adaptor proteins, which induce specific cellular responses (Cook et al., 2014; Hanna and El-Sibai, 2013; Hodge and Ridley, 2016; Schaefer et al., 2014). Rho GDIs are non-enzymatic cytosolic chaperone proteins that keep Rho GTPases in their GDP-bound inactive state (Hanna and El-Sibai, 2013; Schaefer et al., 2014). Rho GDIs are able to do this by blocking the hydrophobic domains of Rho GTPases and by preventing their translocation to the plasma membrane, where they are often activated, and thereby preventing the GDP to GTP exchange (Cook et al., 2014; Hanna and El-Sibai, 2013; Schaefer et al., 2014). Rho GDIs can also

act as positive regulators and maintain Rho GTPases in their active GTP-bound state through GAP inhibition (Ota et al., 2015).

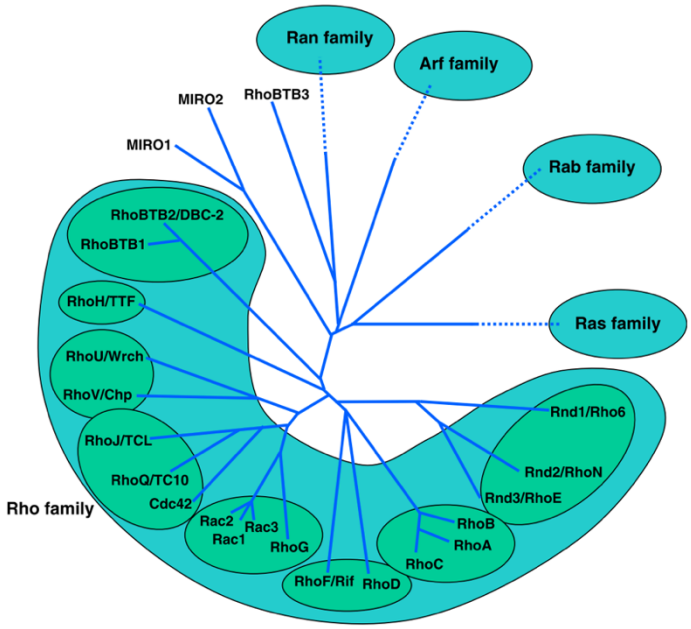

Figure 1. Phylogenetic tree showing the Ras superfamily of small GTPases. There are 20 human members of Rho GTPases (circled and coloured in green) and 8 subfamilies (circled and coloured in turquoise, as well as MIRO1, MIRO2, and RhoBTB3). Adapted from Vega & Ridley, 2008.

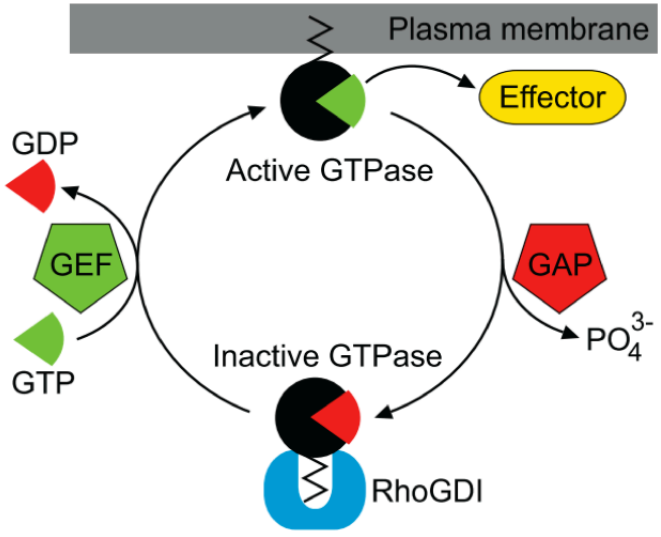

Figure 2. Rho GTPases cycle between active and inactive forms. GEFs activate Rho GTPases by exchanging GDP to GTP. They are then targeted to the membrane where they interact with effector proteins. Rho GTPases are inactivated by GAPs through GTP hydrolysis. Rho GDIs retain the Rho GTPase in the cytoplasm in an inactive GDP-bound form. Adapted from Fritz & Pertz, 2016.

1.2.2 The structure of Rho GTPases

Rho GTPases share a G-domain, a highly conserved structure present in many guanine nucleotide-binding proteins, that is responsible for guanine nucleotide binding and hydrolysis (Cherfils and Zeghouf, 2013; Hodge and Ridley, 2016; Paduch et al., 2001; Vetter and Wittinghofer, 2001). The G-domain is made up of five α-helices (A1 – A5), six-stranded β-sheets (B1 – B6), and five polypeptide loops (G1 – G5), (Cherfils and Zeghouf, 2013; Hodge and Ridley, 2016; Paduch et al., 2001; Vetter and Wittinghofer, 2001).

The G1 loop, known as the phosphate-binding loop (P-loop), binds the phosphate groups of the guanine nucleotide with the help of a conserved GXXXXGKS/T motif (Cherfils and Zeghouf, 2013; Hodge and Ridley, 2016; Paduch et al., 2001; Vetter and Wittinghofer, 2001). G2 and G3 correspond to the switch I and switch II regions, respectively, and switching between GDP and GTP involves these two switch regions, since they are both bound to the γ-phosphate of the nucleotide (Cherfils and Zeghouf, 2013; Paduch et al., 2001). In the GTP bound form, the NH group of threonine in switch I and the NH group of glycine in switch II are bound to the oxygens of the γ-phosphate, and switch I and II are in a more "tense" conformation. When GTP is hydrolyzed, this tense conformation changes to a more relaxed one, and this change in conformation from tense to relaxed is often called the "loaded spring" mechanism (**Figure 3**), (Cherfils and Zeghouf, 2013; Vetter and Wittinghofer, 2001). Both G4 and G5 recognize the guanine base. G4 has a conserved N/TKXD motif that interacts with the guanine nucleotide whereas G5 recognizes the guanine base (Cherfils and Zeghouf, 2013; Paduch et al., 2001).

At the C-terminus of the G-domain, there is a hypervariable domain which includes polybasic amino acid residues, and a CAAX (C is for cysteine, A is for aliphatic amino acid, X is for any amino acid) motif downstream of this polybasic region, both of which give Rho GTPases

their specificity (**Figure 4**), (Hodge and Ridley, 2016; Roberts et al., 2008). The polybasic region mainly contains positively charged lysine and arginine residues, allowing it to interact with the plasma membrane (Hodge and Ridley, 2016; Roberts et al., 2008). The recognition of the CAAX motif is what initiates posttranslational modifications (PTMs), and PTMs are important for ensuring that Rho GTPases are at the correct cellular location (Roberts et al., 2008).

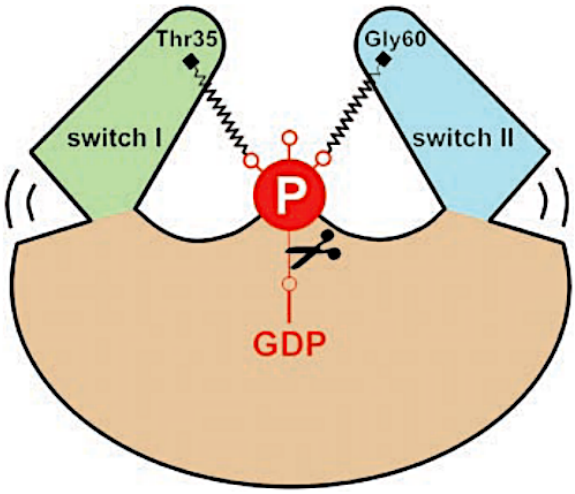

Figure 3. The loaded spring mechanism. In the tense, GTP-bound conformation, threonine in switch I and glycine in switch II are bound to the γ-phosphates of the guanine nucleotide. When GTP is hydrolyzed, the conformation changes to a more relaxed state. Adapted from Vetter & Wittinghofer 2001.

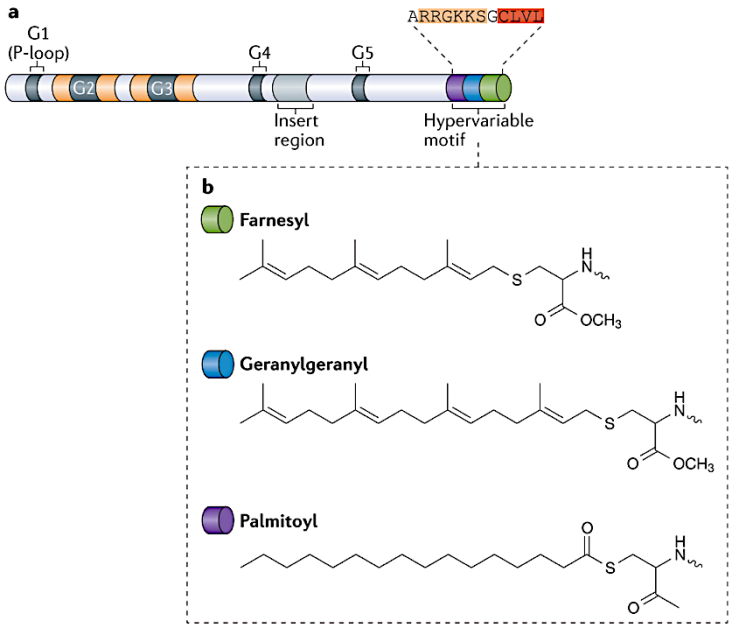

Figure 4. Rho GTPase structure. **(a)** At the C-terminus, the polybasic region is highlighted in orange and the CAAX motif is highlighted in red. The CAAX motif undergoes posttranslational lipid modifications that help target Rho GTPases to membranes. Isoprenylation is the most common type of lipid modification and includes farnesylation (green), geranylgeranylation (blue), and palmitoylation (purple). **(b)** Chemical structure of farnesyl, geranylgeranyl, and palmitoyl groups. Adapted from Hodge & Ridley, 2016.

1.2.3 Posttranslational modifications (PTMs) of Rho GTPases

Lipid modifications, phosphorylation, sumoylation, and ubiquitylation are the four main PTMs by which Rho GTPases are regulated, (**Figure 4**), (Hodge and Ridley, 2016). Since Rho GTPases need to be localized to membranes in order to be activated by Rho GEFs, lipid modifications are necessary to achieve this (Hodge and Ridley, 2016; Roberts et al., 2008). Two such known are prenylation, which increases hydrophobicity and aids in membrane targeting, and S-palmitoylation (Hodge and Ridley, 2016; Roberts et al., 2008). In prenylation, an isoprenoid group, made of 5-carbon isoprene units, is attached to a cysteine residue in the CAAX motif. For Rho GTPases, farnesyltransferase and geranylgeranyltransferase add a farnesyl or geranylgeranyl isoprenoid lipid, respectively, to the cysteine residue (Hodge and Ridley, 2016; Roberts et al., 2008). After these are added, an endoprotease called Rce1 (Ras-converting enzyme 1) removes the -AAX portion of the CAAX motif, and a methyl group is added to the now prenylated cysteine residue by isoprenylcysteine-O-carboxyl methyltransferase (Hodge and Ridley, 2016; Roberts et al., 2008). S-palmitoylation occurs when palmitoyltransferase adds a palmitate group to the cysteine residue in the CAAX motif (Hodge and Ridley, 2016). The PTM that takes place depends on the amino acid (X) present in the CAAX motif (Foster et al., 1996). For example, if the amino acid is leucine or phenylalanine, a geranylgeranyl group will be added, whereas if the amino acid is methionine, serine, alanine, cysteine or glutamine, a farnesyl group will be added (Foster et al., 1996).

Phosphorylation can have multiple effects on Rho GTPases; phosphorylation can alter Rho GTPase activity by affecting guanine nucleotide binding, and thereby the cycling between active and inactive forms (Hodge and Ridley, 2016). Rho GTPases can also be kept in their inactive forms in the cytosol by Rho GDIs, since phosphorylation can signal the removal of Rho GTPases from

the plasma membrane, where they are usually activated (Hodge and Ridley, 2016). Phosphorylation can also change Rho GTPase localization, as well as target them for degradation (Hodge and Ridley, 2016).

Ubiquitylation and sumoylation are similar processes due to the fact that they both use an E1 activating, E2 conjugating, and E3 ligase enzymes to alter Rho GTPases (Hodge and Ridley, 2016). The protein is marked for degradation when polyubiquitylation on Lys48 residues occurs (Hodge and Ridley, 2016). When poly- or monoubiquitylation occurs on other lysine residues (other than Lys48), proteins may be brought to different cellular compartments, or initiate DNA repair mechanisms (Hodge and Ridley, 2016). Sumoylation is linked to transcriptional regulation and nuclear transport. Small ubiquitin-related modifiers (SUMOs) become mature when they are processed by sentrin-specific proteases. This mature SUMO eventually ends up on a lysine residue in the target protein and is thereby able to affect transcriptional processes and nuclear transport (Hodge and Ridley, 2016).

1.2.4 Atypical Rho GTPases

Atypical Rho GTPases are not molecular switches, meaning that they do not cycle between active and inactive forms like the classical Rho GTPases (Aspenström, 2018; Aspenström et al., 2007). They are not known to be regulated by GEFs or GAPs, but can be regulated by PTMs, localization, degradation, and by interactions with other proteins (Aspenström et al., 2007; Chardin, 2006). Atypical Rho GTPases are for the most part always bound to GTP (Hodge and Ridley, 2016). They can be either GTPase deficient or fast-cycling (Aspenström, 2018; Aspenström et al., 2007). Due to amino acid substitutions at specific sites required for GTP hydrolysis, GTPase deficient Rho GTPases are unable to hydrolyze GTP, and are therefore constitutively active (Aspenström, 2018; Aspenström et al., 2007). On the other hand, fast-cycling Rho GTPases cycle through GTP and GDP so quickly that GTP hydrolysis does not get the chance to take place, and since there is more GTP than GDP in the cell, this makes fast-cycling Rho GTPases essentially constitutively GTP-bound (Aspenström, 2018).

1.2.5 Rho GAPs

The process of inactivation of Rho GTPases through the hydrolysis of GTP is slow, but is sped up with the help of Rho GTPase-activating proteins (Rho GAPs), (Bos et al., 2007; Paduch et al., 2001; Vetter and Wittinghofer, 2001). The Ras-RasGAP complex was first used to study the acceleration of GTP hydrolysis due to a GAP. Although Ras GAPs are structurally unrelated to Rho GAPs, a similar mechanism was found to be in place in the latter (Bos et al., 2007). When switch I and switch II regions of the Rho GTPase interact with the GAP, a conformational change is induced and a transition towards an intermediate hydrolytic reaction state is favoured. The arginine finger provided by the GAP stabilizes the transition state and helps to ensure that the glutamine residue in switch II is properly aligned with a water molecule. Once the water molecule is activated by the glutamine residue, the γ-phosphate of GTP can undergo a nucleophilic attack (Bos et al., 2007; Cherfils and Zeghouf, 2013; Paduch et al., 2001).

1.2.6 Rho GEFs

The two families of Rho guanine nucleotide exchange factors (Rho GEFs) each have at least two domains in common: a catalytic domain, and a domain that helps targeting Rho GEFs to the plasma membrane where they can activate Rho GTPases (Van Buul et al., 2014; Goicoechea et al., 2014; Paduch et al., 2001; Schmidt and Hall, 2002). The Dbl family, which consists of the majority of Rho GEFs, has a Dbl homology (DH) domain with three conserved regions (CR1, CR2, CR3) within it that help with GTPase interaction and catalysis. Adjacent to the DH domain is the pleckstrin homology (PH) domain responsible for plasma membrane localization (Van Buul et al., 2014; Goicoechea et al., 2014; Paduch et al., 2001; Schmidt and Hall, 2002). The PH domain can also have other regulatory roles, such as autoinhibition of the DH domain, and signal specificity, due to its ability to assume more flexible positions than the DH domain (Cherfils and Zeghouf, 2013). The DOCK (Dedicator of Cytokinesis) family of Rho GEFs, similar to the Dbl family, also has a catalytic DOCK Homology Region 2 (DHR2) domain and a membrane-targeting DOCK Homology Region 1 (DHR1) domain (Cherfils and Zeghouf, 2013; Goicoechea et al., 2014). Like Rho GAPs, the process of activating Rho GTPases (exchanging GDP for GTP) is also slow, and is sped up by Rho GEFs (Bos et al., 2007; Cherfils and Zeghouf, 2013; Vetter and Wittinghofer, 2001). When a Rho GEF is bound, the P-loop is disrupted, which is important for maintaining strong nucleotide binding. This decreases GDP affinity (Bos et al., 2007; Vetter and Wittinghofer, 2001).

1.2.7 Rho GTPases in single cell migration

Autonomous cell migration can be described as a cyclical process (Horwitz and Webb, 2003; Ilina and Friedl, 2009; Ridley et al., 2003; Zegers and Friedl, 2014) resulting from the spatial and temporal regulation of Rho GTPases and their effectors, (**Figure 5**) (Horwitz and Webb, 2003). Cells first polarize, and extend protrusions through actin polymerization, regulated by Rac and Cdc42 (Ilina and Friedl, 2009; Ridley et al., 2003). Rac is known to form broad, sheet-like protrusions called lamellipodia and Cdc42 forms spiked protrusions consisting of actin bundles arranged in parallel (Ridley et al., 2003; Zegers and Friedl, 2014).

Effectors of Rac and Cdc42 that help in generating and maintaining protrusions at the cell front are the WASP family of proteins (WASP and WAVE), and p21 activating kinase (PAK), a serine/threonine kinase (Devreotes and Horwitz, 2015; Hanna and El-Sibai, 2013; Ridley, 2011). Rac1 interacts with WAVE whereas Cdc42 interacts with WASP, and both WASP and WAVE are able to activate the Arp2/3 complex which is responsible for actin nucleation and polymerization (**Figure 6**, **Figure 7**) (Devreotes and Horwitz, 2015; Ridley et al., 2003). The process of actin polymerization can be sped up through the binding of WASP and WAVE to profilin (**Figure 7**) (Raftopoulou and Hall, 2004; Ridley et al., 2003). Profilin works together with Arp2/3 and helps target actin monomers to growing ends of actin filaments (Devreotes and Horwitz, 2015; Raftopoulou and Hall, 2004; Ridley et al., 2003). PAK is an effector common to both Rac1 and Cdc42 (Hanna and El-Sibai, 2013). PAK activation by either Rac1 or Cdc42 leads to LIM kinase (LIMK) activation, and then LIMK phosphorylates and inactivates cofilin. Cofilin normally cleaves actin filaments, and thus this inactivation stabilizes actin filaments (Devreotes and Horwitz, 2015; Llense and Etienne-Manneville, 2015). In order for novel actin networks to form for future protrusions, cofilin would need to be activated by Slingshot, a phosphatase located at

the back of lamellipodia, so that cofilin can then disassemble actin filaments and provide actin monomers (Llense and Etienne-Manneville, 2015; Ridley et al., 2003; Zegers and Friedl, 2014). PAK can also help in preventing actomyosin contractility by phosphorylating and inactivating myosin light chain kinase (MLCK), which then cannot activate myosin light chain (MLC), inhibiting actomyosin contractility (**Figure 6**), (Hanna and El-Sibai, 2013). In addition to Rac/Cdc42 and PAK, another way LIMK can be activated is via Rho/ROCK signalling (**Figure 6**), (Bernard, 2007; Hanna and El-Sibai, 2013). Although both these pathways affect the actin cytoskeleton (Devreotes and Horwitz, 2015; Hanna and El-Sibai, 2013), LIMK has been shown to have an effect on microtubules as well, although the mechanism for this is not clear (Prunier et al., 2017). For example, the Rho-ROCK-LIMK pathway is important for the formation of astral microtubules (Prunier et al., 2017).

Filopodia, like lamellipodia, are actin structures formed with the help of formins (Llense and Etienne-Manneville, 2015; Ridley, 2011; Zegers and Friedl, 2014). Formins like mammalian Diaphanous (mDia)1 and mDia2 promote actin polymerization (Llense and Etienne-Manneville, 2015; Ridley, 2011; Zegers and Friedl, 2014). However, additional proteins take part in their polymerization; Fascin, which arranges actin filaments in bundles, helps give filopodia the stiffness they need to move through the plasma membrane outwards, (**Figure 8**) (Ridley, 2015; Ridley et al., 2003). IRSp53 is another protein that interacts with Cdc42 that helps in plasma membrane protrusion with the help of its I-BAR domain (Ridley, 2011). Both lamellipodia and filopodia use VASP and associated proteins, which concentrate at the barbed ends of actin filaments, and lengthen the filaments by adding actin monomers (Ridley, 2011).

After these protrusions by Rac and Cdc42 are formed, the cell then adheres to the substrate through integrins, forming nascent adhesions, or focal complexes, at the front of the cell (Lawson

and Burridge, 2014; Llense and Etienne-Manneville, 2015; Ridley et al., 2003). These adhesions support lamellipodia and give the cell traction, allowing it to move forward, (**Figure 5**), (Devreotes and Horwitz, 2015; Ridley et al., 2003). At the rear of the cell, adhesions disassemble. This can be due to increased tension between integrins and the substrate, or through calpain, a protease activated by calcium, which is released by mechanosensitive calcium channels. Calpain then cleaves these focal adhesions (Devreotes and Horwitz, 2015; Llense and Etienne-Manneville, 2015). After disassembly, actomyosin retraction, regulated by Rho, allows the cell to move forward (Ilina and Friedl, 2009; Zegers and Friedl, 2014). Effectors downstream of Rho such as Rho kinase (ROCK), and MLCK help with actomyosin contractility, (**Figure 5**, **Figure 6**) (Hanna and El-Sibai, 2013; Ridley et al., 2003; Zegers and Friedl, 2014). Rho activates ROCK, which then phosphorylates and activates MLC to activate myosin II (Hanna and El-Sibai, 2013; Ridley et al., 2003). ROCK also phosphorylates and inhibits MLC phosphatase, leading to increased levels of phosphorylated and active MLC (Hanna and El-Sibai, 2013; Ridley et al., 2003).

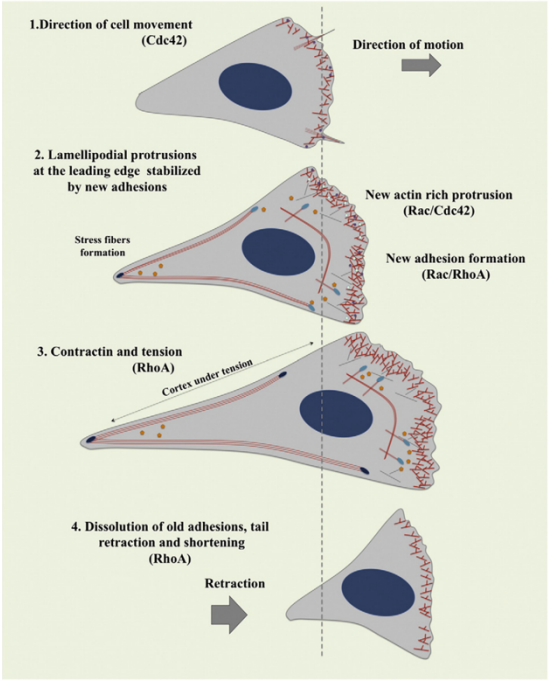

Figure 5. The cyclical process of single cell migration. Rac and Cdc42 localize to the front of the cell, Rho localizes to the back and induces actomyosin contractility. Adapted from Hanna & El-Sibai, 2013.

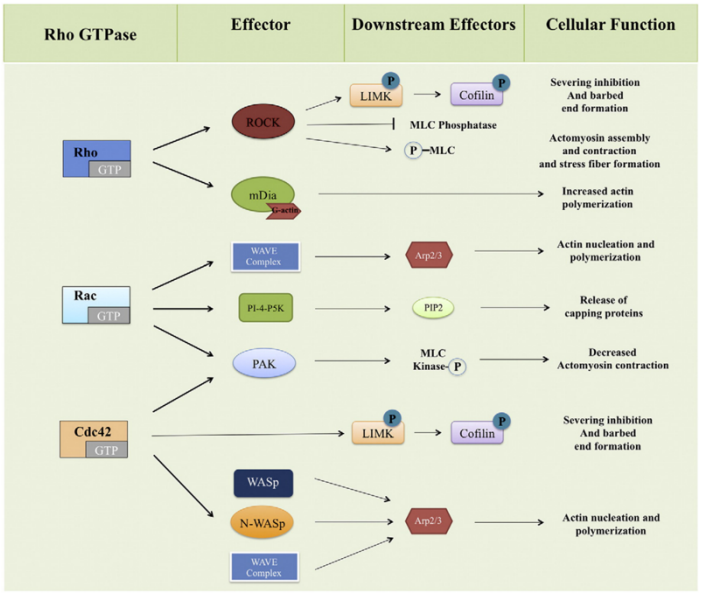

Figure 6. Rho GTPases and their various downstream effectors. Rac interacts with WAVE and Cdc42 interacts with WASP and both can activate the Arp2/3 complex. Both Rac and Cdc42 have PAK as an effector. PAK can inhibit actomyosin contractility by inactivating MLCK. Downstream Rho effectors include ROCK and induce actomyosin contractility. Adapted from Hanna & El-Sibai, 2013.

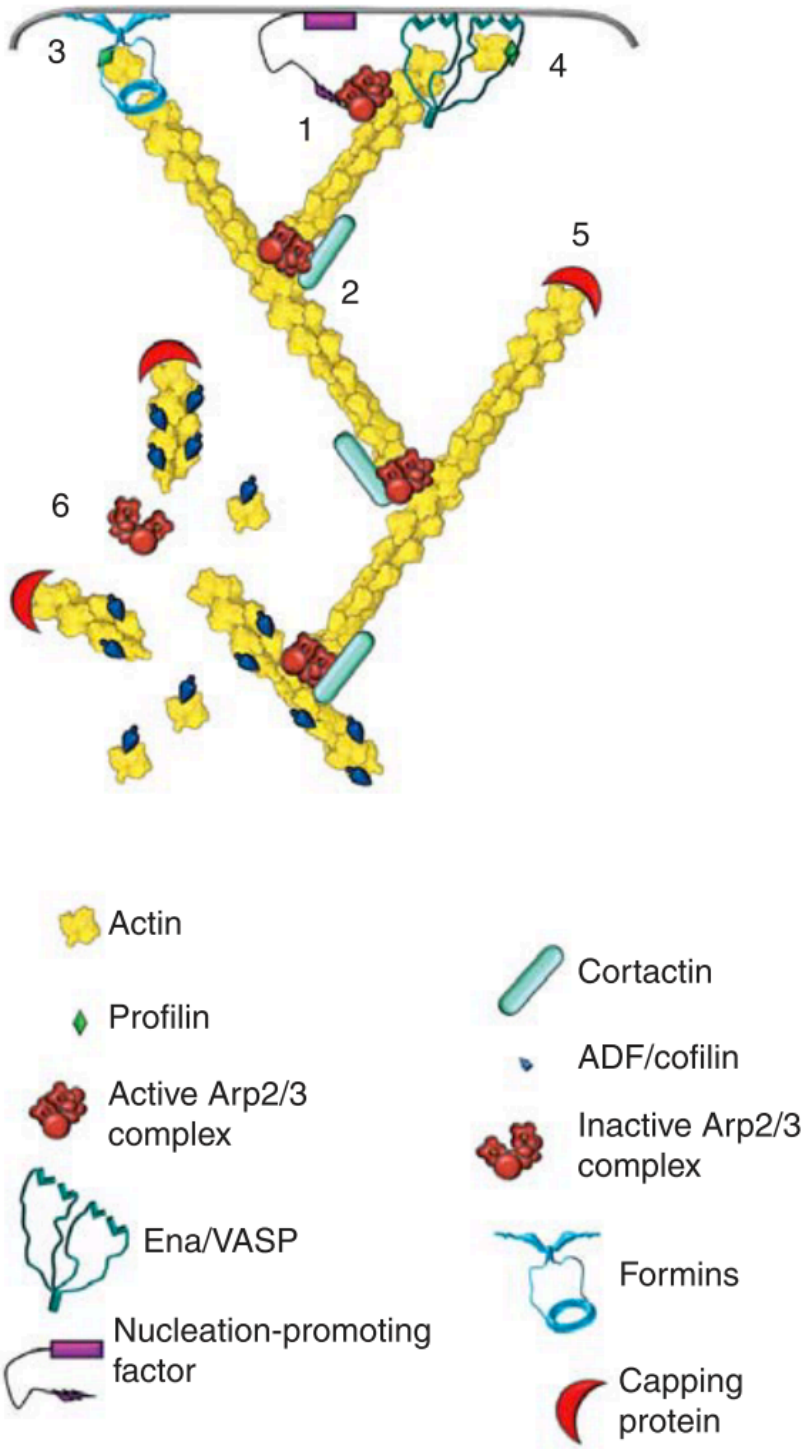

Figure 7. Schematic of lamellipodia formation. **(1)** A nucleation-promoting factor activates the Arp2/3 complex. **(2)** Arp2/3 nucleates new actin filaments and generates branched actin networks. Cortactin helps stabilize actin filaments. Profilin helps target actin monomers to growing ends of actin filaments. Formins **(3)** promote actin polymerization and Ena/VASP proteins **(4)** help elongate actin filaments. **(5)** After elongation, capping proteins cap the growing end of the actin filament. **(6)** Cofilin severs actin filaments. Adapted from Svitkina, 2018.

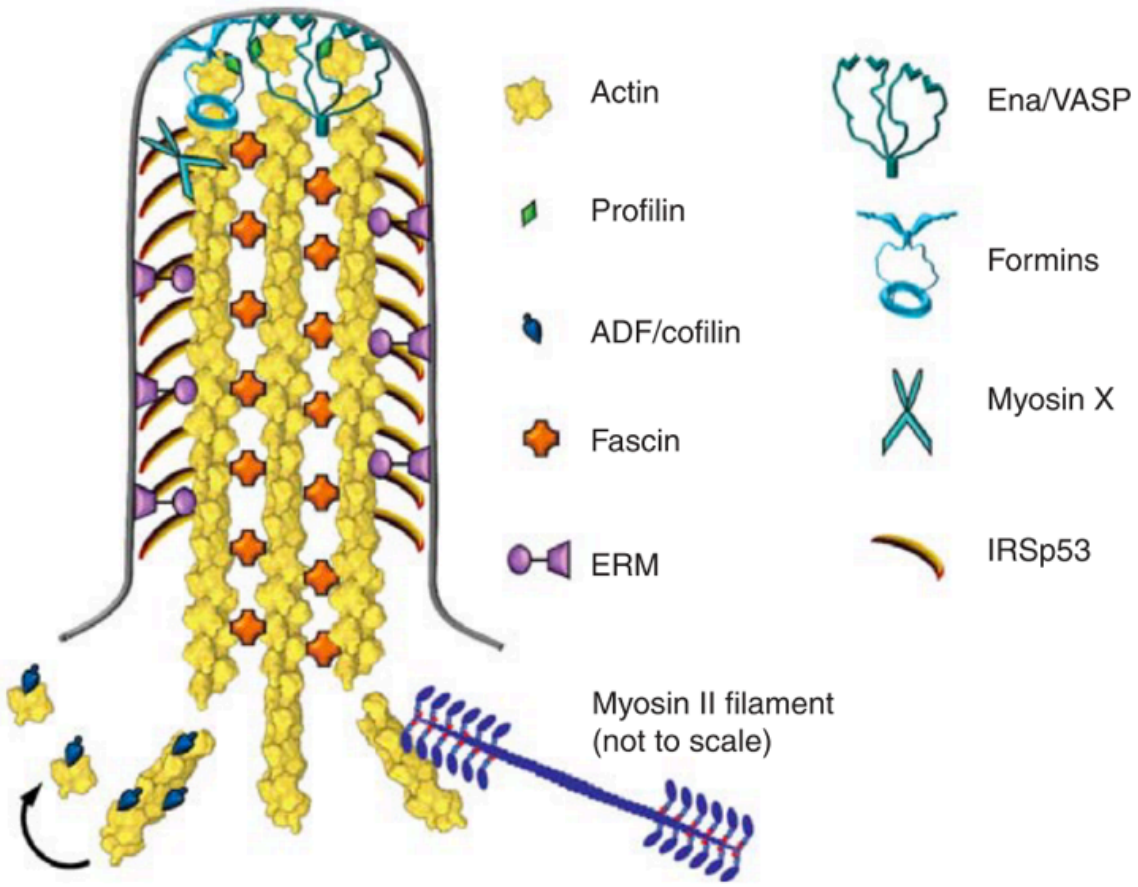

Figure 8. Schematic of filopodia formation. IRSp53 bends the membrane, helps prepare for filopodia formation, and maintains filopodial shape. Fascin bundles actin filaments and ERM (ezrin-radixin-moesin) proteins attach them laterally to the plasma membrane. Profilin helps target actin monomers to growing ends of actin filaments. Formins promote actin polymerization and Ena/VASP proteins help elongate actin filaments. Actin-depolymerizing factor (ADF)/cofilin and myosin II sever actin filaments to create actin monomers that can be recycled. Adapted from Svitkina, 2018.

1.2.8 The regulation of cell adhesions

Adhesions are polarized in migrating cells; nascent adhesions are localized at the front and are frequently turned over, whereas mature and stronger adhesions localize to the back (Lawson and Burridge, 2014). Focal adhesions are structures that help anchor the cell to its substrate (Huttenlocher et al., 1995). They not only serve as traction points, but can also affect cell speed depending on their strength (Huttenlocher et al., 1995). Integrins, which are transmembrane protein receptors consisting of α and β subunits, are major components of focal adhesions, providing a physical link between the cell and its substrate, but they are also signalling hubs activating downstream intracellular pathways (Devreotes and Horwitz, 2015; Huttenlocher et al., 1995). Ligand-binding to integrins induces a conformational change and leads to integrin clustering, which forms nascent adhesions (Llense and Etienne-Manneville, 2015; Ridley et al., 2003). Nascent adhesions are less stable and form at early stages of adhesion, which either mature into more stable focal adhesions, or disassemble (Lawson and Burridge, 2014). These nascent adhesions remain stable due to Rac activation and a suppression of Rho (Lawson and Burridge, 2014). The focal adhesion targeting (FAT) domain of focal adhesion kinase (FAK) binds adaptor proteins such as paxillin and talin, which all help target FAK to focal adhesions, (**Figure 9**), (Scheswohl et al., 2008). Other adaptor proteins localized to focal adhesions include vinculin, Crk, and p130Cas (Huttenlocher et al., 1995). FAK autophosphorylation is induced, and binding sites for proteins with SH2 domains, such as Src (a kinase), are created (Bolós et al., 2010; Lawson and Burridge, 2014; Scheswohl et al., 2008). Src phosphorylation of FAK induces the phosphorylation and activation of paxillin and p130Cas (Lawson and Burridge, 2014; Scheswohl et al., 2008). Paxillin and p130Cas then bind to proteins that help recruit Rac GEFs (one of them being β-PIX), inducing Rac activation, (**Figure 9**), (Lawson and Burridge, 2014). While Rac is being activated,

Rho is being suppressed via p190RhoGAP (Lawson and Burridge, 2014). The formation of mature adhesions at later stages involves the opposite effect; an increase in Rho activity and a suppression of Rac (Lawson and Burridge, 2014). p190RhoGEF activates Rho and induces stress fiber formation, whereas Rac can be suppressed through two different ways (Lawson and Burridge, 2014). A GAP called FilGAP can be activated via ROCK phosphorylation to inhibit Rac, or actomyosin contractility regulated by Rho can inhibit the Rac GEF β-PIX (Lawson and Burridge, 2014). Increased contractility can also spatially segregate Rac and its GEFs, preventing its activation at later stages (Lawson and Burridge, 2014).

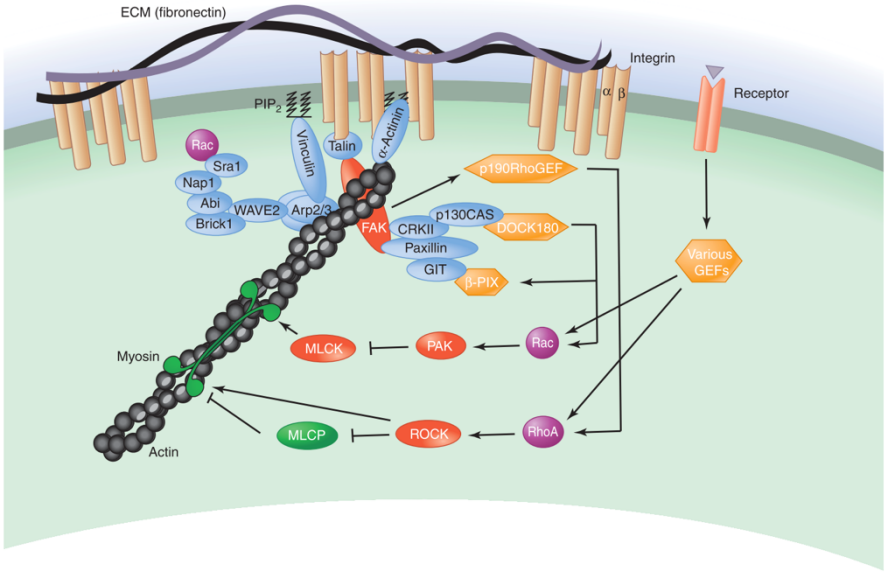

Figure 9. Integrins are major components of focal adhesions. They serve as a signalling hub that activates downstream pathways. Proteins like p130Cas and paxillin bind to FAK. Induction of FAK autophosphorylation causes Src (a kinase) binding. Src phosphorylates FAK which phosphorylates and activates paxillin and p130Cas. GEFs such as β-PIX are recruited which induces Rac activation. Adapted from Devreotes & Horwitz, 2015.

1.2.9 Signalling pathways at the front and rear of cells

Front-back polarity in cells is established through the polarization of Rho GTPases (Llense and Etienne-Manneville, 2015). In order for cells to migrate efficiently, lamellipodia need to be confined to specific cellular regions (Ridley, 2015).

Cdc42 regulates actin polymerization by recruiting Rac to leading edges through microtubule capture and vesicle trafficking (Llense and Etienne-Manneville, 2015; Ridley, 2015), but also by limiting the area of lamellipodia formation (Ridley et al., 2003). Cdc42 does this by rearranging the microtubule organizing center (MTOC) and the Golgi apparatus so that they are in front of the nucleus and facing the cell front (Llense and Etienne-Manneville, 2015; Ridley et al., 2003). Ensuring these structures face the anterior help to guide microtubules towards this part of the cell (MTOC) and ensure that essential cargo from the Golgi, such as proteins necessary for protrusion, get to the front of the cell by using these microtubules as tracks (Ridley et al., 2003).

A positive feedback loop involving phosphoinositides helps sustain Rac and Cdc42 activation and cell protrusions (Llense and Etienne-Manneville, 2015). In regions where there is Rac activity, there is often little or no Rho activity; this is because Rac and Rho inhibit each other, (**Figure 10**), (Llense and Etienne-Manneville, 2015; Mayor and Carmona-Fontaine, 2010; Zegers and Friedl, 2014).

The formation of PIP_3 from PIP_2 via PI3K activates Rac and Cdc42 GEFs, as well as effectors (Devreotes and Horwitz, 2015; Hanna and El-Sibai, 2013; Llense and Etienne-Manneville, 2015). In order for more PIP_3 to be formed, actin polymerization needs to be maintained via Rac so that PI3K remains stabilized. This preserves Rac and Cdc42 at the leading edge and maintains protrusions (Llense and Etienne-Manneville, 2015). Other ways Rac and Cdc42 remain active at the leading edge is via Smurf1, a ubiquitin ligase activated by Par6 and

atypical protein kinase C (aPKC), that degrades Rho (Zegers and Friedl, 2014). Rac can also inactivate Rho by activating p190RhoGAP (Zegers and Friedl, 2014).

Rho can limit Rac activity by activating FilGAP, as mentioned above, or through ROCK activation which prevents the GEF β-PIX from activating Rac and Cdc42 (Zegers and Friedl, 2014). Surprisingly, Rac can also inhibit its own activity via an Arp2/3 inhibitor called Arpin (Ridley, 2015).

Rho GTPase fluorescence resonance energy transfer (FRET) biosensors have been used to determine the spatial and temporal patterns of Rho GTPase activities in cells. Recently, they allowed to determine that Rho does not strictly localize to the rear of the cell (Lawson and Burridge, 2014). For example, Syx, a Rho GEF, can bring Rho to mDia and can contribute to actin polymerization (Lawson and Burridge, 2014; Raftopoulou and Hall, 2004). Another way Rho may promote actin polymerization is through ROCK inhibition via adhesions (Lawson and Burridge, 2014). When adhesions are formed, tyrosine phosphorylation of ROCK mediated by integrins forces Rho to activate mDia instead (Lawson and Burridge, 2014).

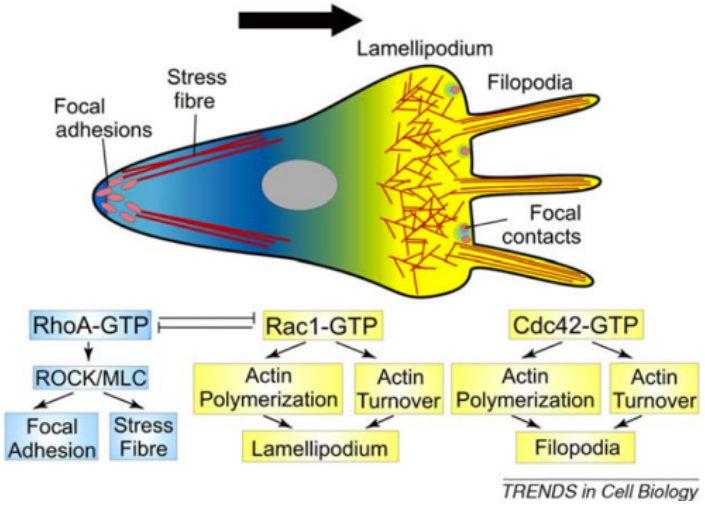

Figure 10. Polarization of the main Rho GTPases involved in cell migration. Rac and Cdc42 localize to the cell front and generate actin protrusions, Rho localizes to the back and regulates stress fibre formation. Rac and Rho inhibit each other. Adapted from Mayor & Carmona-Fontaine, 2010.

1.2.10 Cell-cell adhesions

The intercellular junctions that link cells together in tissues are formed by transmembrane proteins, and their cytoplasmic portions are indirectly linked to actin via cytoplasmic, adaptor, scaffolding, and signalling proteins (Bazzoni and Dejana, 2004; Dejana, 2004; Ebnet et al., 2018; Steinbacher and Ebnet, 2018). This indirect link to actin allows junctions to be stabilized and may help maintain cell shape and polarity (Bazzoni and Dejana, 2004; Dejana, 2004).

The two major junction types present in endothelial cells are adherens junctions and tight junctions (Bazzoni and Dejana, 2004; Cerutti and Ridley, 2017). Adherens junctions are formed primarily by cadherins, which are calcium-dependent transmembrane adhesion proteins (Bazzoni and Dejana, 2004; Dejana et al., 1995; Friedl and Mayor, 2017). Vascular endothelial (VE)-cadherin is expressed specifically in endothelial cells (Bazzoni and Dejana, 2004; Cerutti and Ridley, 2017; Dejana et al., 1995). Through its cytoplasmic domain, VE-cadherin is indirectly bound to actin via cytoplasmic proteins such as α-, β-, and γ-catenin (also known as plakoglobin), p120-catenin, vinculin, and α-actinin (Cerutti and Ridley, 2017; Dorland and Huveneers, 2016; Friedl and Mayor, 2017). β- and γ-catenin are directly bound to the intracellular portion of VE-cadherin, which is then bound to α-catenin, and then α-catenin is bound to actin (Bazzoni and Dejana, 2004). α-actinin and vinculin can also bind to α-catenin for further stability of the adherens junction-actin linkage (Bazzoni and Dejana, 2004). Other proteins associated with VE-cadherin include VE-PTP, which regulates phosphorylation of cadherins and catenins (Dejana, 2004), and PECAM-1, which retains endothelial cells together and contributes to junctional support, (**Figure 11**), (Cerutti and Ridley, 2017; Dejana et al., 1995).

Tight junctions are complexes composed of transmembrane proteins such as occludin, claudins, and junctional adhesion molecules, (Cerutti and Ridley, 2017; Friedl and Mayor, 2017).

They form tough barriers and regulate cell monolayer permeability, ensuring that only ions and solutes of a certain size can pass through (Bazzoni and Dejana, 2004; Cerutti and Ridley, 2017; Dejana, 2004; Friedl and Mayor, 2017; Rahimi, 2017). Just like in adherens junctions, tight junctions are indirectly connected to the actin cytoskeleton through zonula occludens proteins and cingulin, which bind to the cytoplasmic side of tight junctions (**Figure 11**), (Cerutti and Ridley, 2017; Dejana et al., 1995; Steinbacher and Ebnet, 2018).

A protein complex that has been found to be part of both adherens junctions and tight junctions in the nectin-afadin complex (**Figure 11**), (Bazzoni and Dejana, 2004; Dejana, 2004). Nectins are a family of cell adhesion molecules bound to afadin, which helps indirectly to connect nectins to actin (Bazzoni and Dejana, 2004; Dejana, 2004). In adherens junctions, afadin is bound to ponsin and α-catenin whereas in tight junctions, afadin can interact with junctional adhesion molecules and nectins with zonula occludens proteins (Bazzoni and Dejana, 2004; Dejana, 2004).

Another type of adhesion molecule in endothelial cells are membrane channels called gap junctions (Bazzoni and Dejana, 2004; Friedl and Mayor, 2017). Gap junctions are formed by connexins that are organized into hydrophilic channels called connexons, and regulate the passage of ions and small molecules (Bazzoni and Dejana, 2004; Dejana et al., 1995; Friedl and Mayor, 2017). Gap junctions not only contribute to intercellular communication, adhesion, and junction stability, but can also influence coordination and cell cohesion during collective cell migration (Bazzoni and Dejana, 2004; Friedl and Mayor, 2017).

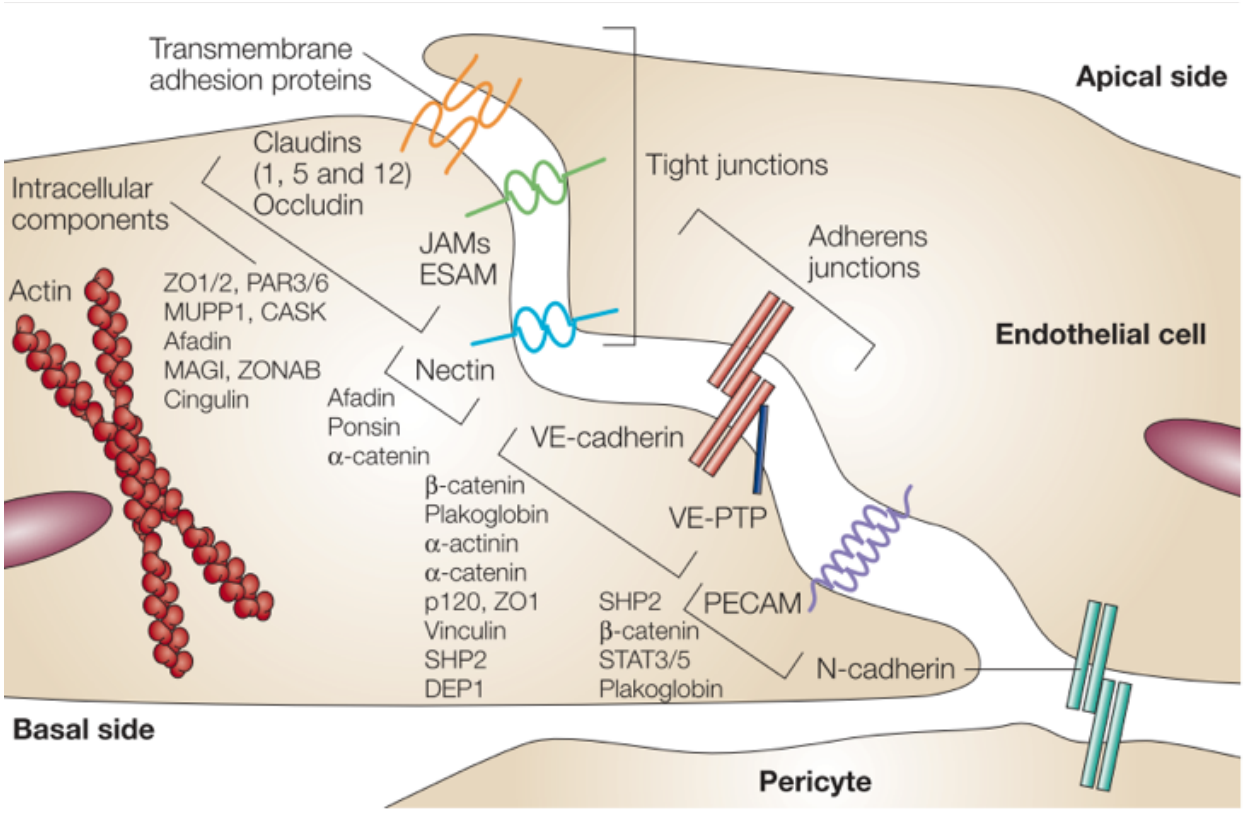

Figure 11. Overview of the various cell-cell junction complexes in endothelial cells. Adapted from Dejana, 2004.

1.2.11 Collective cell migration

When cells migrate collectively, each cell within the group follows the same cyclical process as in autonomous cell migration (**Figure 12a**), (Ilina and Friedl, 2009; Mayor and Etienne-Manneville, 2016). Individual cells within the collective can move autonomously by forming "cryptic lamellipodia," with the rest of the cells in the group also possessing these directional protrusions, indicating that signalling across intercellular junctions results in the coordination and polarization of the collective and induces the regulation of Rho GTPases (**Figure 12b**), (Ebnet et al., 2018; Farooqui and Fenteany, 2005; Mayor and Etienne-Manneville, 2016; Steinbacher and Ebnet, 2018).

Structures that ensure that endothelial cell polarity is transmitted to the collective are called cadherin fingers (Hayer et al., 2016). These are extensions of the plasma membrane that appear at the rear of a leader cell and that are engulfed by a follower cell's front end (Hayer et al., 2016). Cadherin fingers are mediated by the VE-cadherin-catenin complex (Hayer et al., 2016). Cadherin fingers help polarize and guide collectively migrating endothelial cells (Hayer et al., 2016).

Within a cell collective, there are leader cells, located at the front, and follower cells, located at the back of leader cells (Mayor and Etienne-Manneville, 2016). Leader cells are able to transmit forces to the follower cells through VE-cadherin-mediated junctions, instructing the latter to follow along (**Figure 12c**) (Ebnet et al., 2018; Mayor and Etienne-Manneville, 2016). Follower cells may use mechanosensing to detect and react to the forces applied by the leader cells, which are transduced through mechanotransducers, proteins that may be part of focal adhesions and adherens junctions (Ebnet et al., 2018; Mayor and Etienne-Manneville, 2016). Examples of mechanotransducers include talin and α-catenin, which act as intermediary links to integrins and

cadherins, respectively, and can relay signals to the actin cytoskeleton of adjacent cells (Mayor and Etienne-Manneville, 2016).

Adhesion strength and stability is regulated through the conformational changes of mechanotransducers (Mayor and Etienne-Manneville, 2016). For instance, when tension is sensed, a conformational change in α-catenin is induced, and vinculin is able to bind (Dorland and Huveneers, 2016; Ebnet et al., 2018; Mayor and Etienne-Manneville, 2016). The presence of vinculin only occurs when there is increased tension across a junction, since vinculin is not recruited when tension levels are low (Dorland and Huveneers, 2016). This increases the stability and strength of α-catenin-actin binding (Dorland and Huveneers, 2016; Ebnet et al., 2018; Mayor and Etienne-Manneville, 2016).

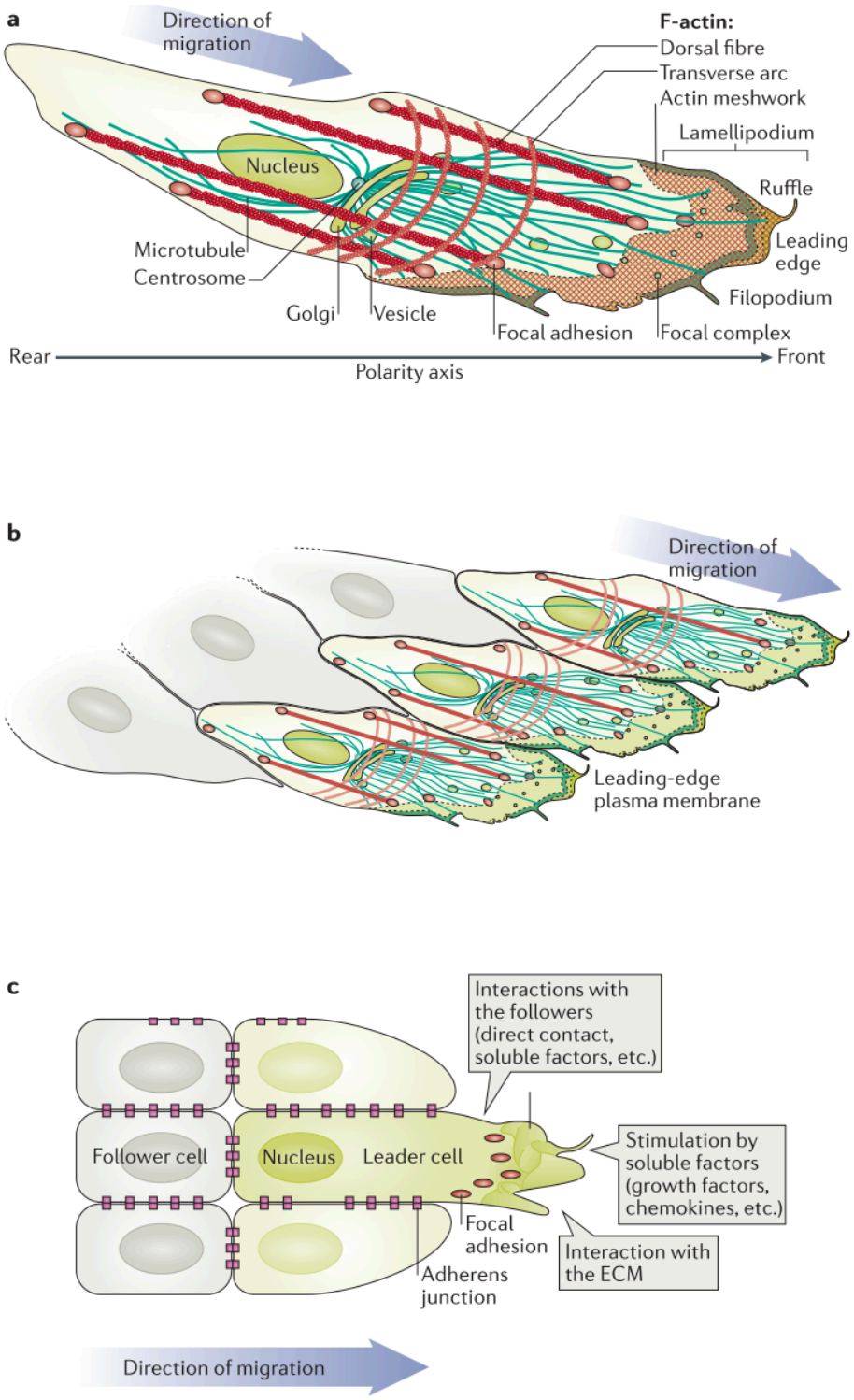

Figure 12. Polarization of structures in single versus collectively migrating cells. **(a)**, **(b)** Individual cells within the collective can move autonomously. Signalling across intercellular junctions results in the coordination and polarization of the collective. **(c)** In a collectively migrating group, leader cells can transmit forces to the follower cells through cell-cell junctions. Adapted from Mayor & Etienne-Manneville, 2016.

1.3 Aim

The way in which Rho GTPase signalling is regulated spatially and temporally during autonomous cell migration, and how cells coordinate their behaviour across intercellular adhesions when migrating as a collective, is not well understood. A previously performed siRNA screen (**Figure 13**) helped identify candidate regulators of collective cell migration (Hayer, unpublished). This screen was done by transfecting HUVECs (Human Umbilical Vein Endothelial Cells) with siRNAs targeting genes coding for either Rho GEFs, Rho GAPs, and Rho GTPases. Cells were tracked and their velocity and coordination was quantified. Coordination was determined by tracking each cell, and measuring their velocity and that of their neighbours within a 100 μm radius, and then taking the average cosine of all the angles between a given cell and all its neighbours (**Figure 14**), (Hayer et al., 2016).

When the resulting cell velocity and coordination phenotypes of all knockdown conditions were plotted against each other, distinct phenotypes emerged (**Figure 13**). In the lower left quadrant, phenotypes with slower migration speed and lower coordination relative to controls are most likely less well coordinated because they move less (lower velocity), i.e. this group of regulators is likely necessary for autonomous cell migration. Phenotypes with higher velocities but low coordination in the bottom right quadrant probably have a defect in mechanical coupling between cells, as this increases the speed of individual cells. Phenotypes displaying lower velocity but higher coordination might be due to cells being more tightly coupled with each other, thereby reducing autonomous movement. No significant phenotypes were observed having both increased coordination and cell velocity.

We decided to follow up on two candidates that generated strong phenotypes: The Rho GEF FARP1 and the atypical Rho GTPase RND3.

FARP1 knockdown caused a decrease in both velocity and coordination, placing it in the bottom left quadrant. Based on the previous explanations, FARP1 may be more involved in regulating autonomous cell migration because of their lower coordination.

RND3 knockdown caused a decrease in velocity, but a large increase in coordination, placing it in the upper left quadrant. From this, RND3 may be linked to the regulation of cell-cell adhesion.

The goal of this project was to validate the candidate regulators FARP1 and RND3 as screening hits and to investigate the molecular mechanisms by which they regulate autonomous and collective cell migration.

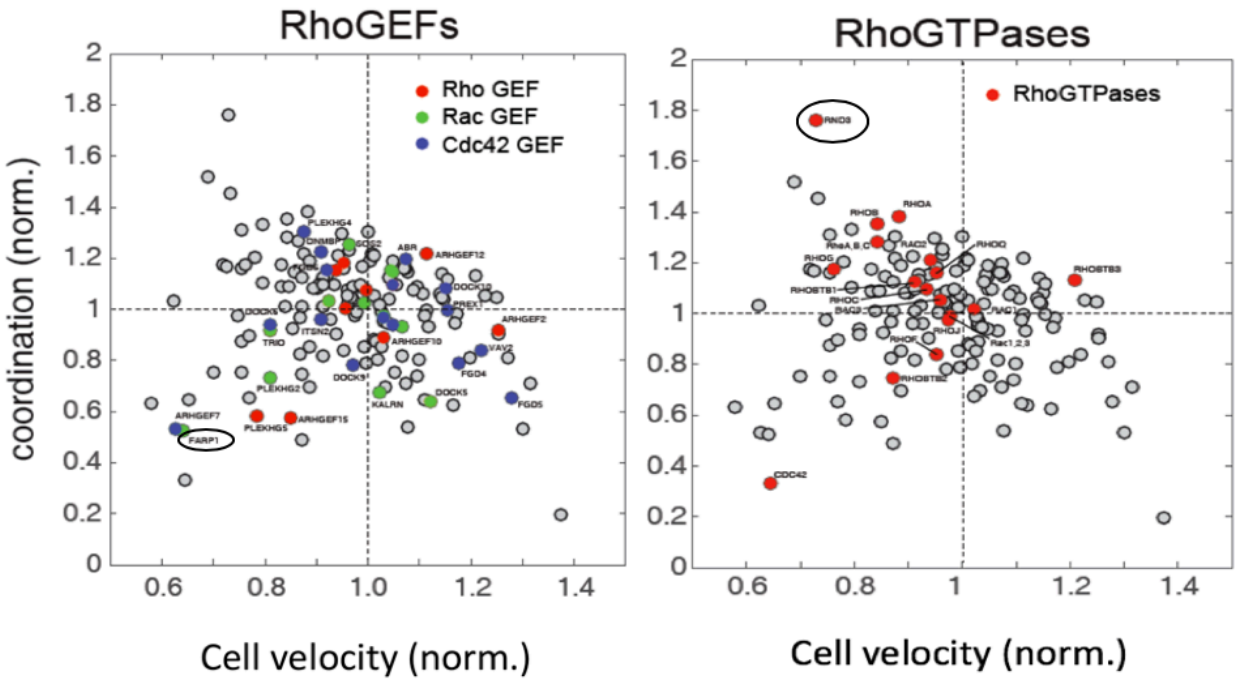

Figure 13. siRNA screen for Rho GEFs and Rho GTPases expressed in endothelial cells (Hayer, unpublished). The Rho GEF FARP1 and the atypical Rho GTPase RND3 (both circled) were identified as candidate regulators of collective cell migration.

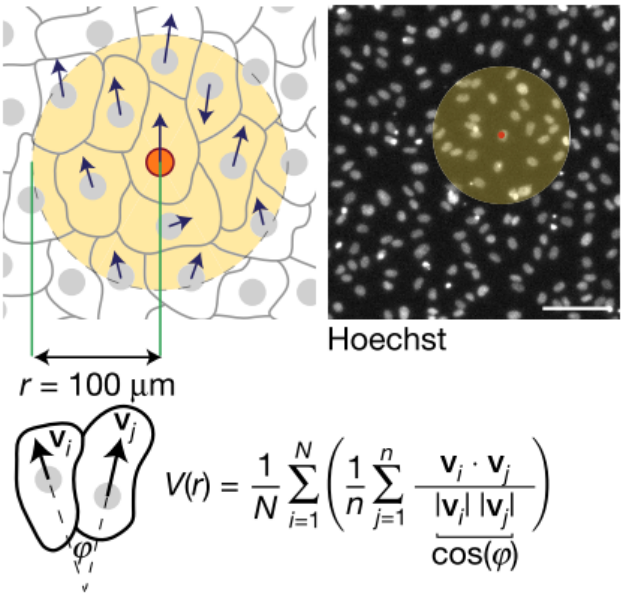

Figure 14. Quantifying coordination. N is the number of cells migrating at velocity V_i and n is the number of neighbours around N (within a 100 µm radius) migrating at velocities V_j. Coordination was determined by tracking cell nuclei, measuring V_i and V_j, and then computing the averaged cosine of the angles. Adapted from Hayer et al., 2016.

1.4 The Rho GEF FARP1

FARP1 is a RhoGEF belonging to the Dbl family of GEFs (He et al., 2013; Kuo et al., 2018). It has a 4.1, ezrin, radixin, moesin (FERM) domain at its N-terminus, and further down from this FERM domain, a DH domain and two PH domains (**Figure 15**), (He et al., 2013; Kuo et al., 2018). These three domains are connected to each other via linkers (He et al., 2013). The catalytic DH domain is blocked via both PH domains and the linkers, indicating that FARP1 exhibits an autoinhibited conformation stabilized by the interaction of all these elements (He et al., 2013; Kuo et al., 2018). For FARP1 to perform as a GEF, conformational changes need to take place so that this autoinhibition is relieved (He et al., 2013; Kuo et al., 2018). Structural studies on FARP2 (a homolog of FARP1 that shares a similar domain structure) revealed a possible mechanism by which this autoinhibition is relieved (He et al., 2013). The phosphorylation of tyrosine residues in the interaction area of DH and the second PH domain (PH2) induces a disruption of the DH-PH2 interaction (He et al., 2013). Although this interaction is disrupted, autoinhibition is still not completely relieved because a portion of an α-helix in the DH domain is still inhibiting the catalytic area (He et al., 2013). Since autoinhibition is not as strong as it was before, this encourages binding of an allosteric activator and ensures full activation of the GEF (He et al., 2013). Based on what is seen in the nectin pathway, it is suggested that Rap (a Ras homolog) is the allosteric activator due to its ability to activate FARP2 (He et al., 2013).

FARP1 localizes to the plasma membrane due to the many positive charges in the FERM domain (Kuo et al., 2018). The FERM domain is imperative for the localization of FARP1 to the membrane, since a truncated version displaced FARP1 to the cytosol (Kuo et al., 2018).

Not only does the FERM domain contain a positively charged Lys-Arg-Lys-Arg (KRKR) motif, but its surface also has polarized electrostatic potential (Kuo et al., 2018). All these positive

charges promote binding to negatively charged phospholipids (Kuo et al., 2018). In support of this, micrographs of FARP1 cellular distribution demonstrate that it indeed localizes to the plasma membrane (Müller et al., 2020).

To understand how FARP1 regulates migration, it is important to know which Rho GTPases it interacts with and activates. FARP1 is promiscuous and seems to interact with Rho, Rac, and Cdc42 (Bagci et al., 2020). For example, FARP1 has been shown to interact with Rho (García-Mata and Burridge, 2007; He et al., 2013). This was also observed in another recent study, however the FARP1-Rho interaction did not surpass activity thresholds, nor was the result significant (Müller et al., 2020). FARP1 was found to mediate endothelial barrier function by interacting with Cdc42 (Amado-Azevedo et al., 2017), whereas it interacts with Rac in neurons to regulate dendritic filopodial dynamics (Cheadle and Biederer, 2012). These conflicting results suggest that FARP1 interactions with Rho GTPases need to be further investigated.

FARP1 has also been studied in pathologies such as tumours and gastric cancer (Croisé et al., 2016, 2017; Hirano et al., 2020). In neuroendocrine tumours called pheochromocytomas, FARP1 expression and Cdc42 activity decreased (Croisé et al., 2016) and it was later shown that this reduction in FARP1 expression was correlated with Cdc42 inhibition (Croisé et al., 2017). In gastric cancer, FARP1 expression encouraged cancer cell motility and invasion and filopodium formation through interaction with integrin αvβ5 and activation of Cdc42 (Hirano et al., 2020). Integrin αvβ5 expression was positively correlated with FARP1 mRNA expression and knocking down this integrin diminished the migratory capabilities of the cancer cells as well as filopodium formation by FARP1 (Hirano et al., 2020). In addition, patients with a high expression of FARP1 did not survive as long as those with lower expression levels (Hirano et al., 2020).

Mitogen-activated kinase kinase kinase kinase 4 (MAP4K4) is a serine/threonine kinase involved in the regulation of endothelial cell migration and cytoskeletal dynamics (Schwaid et al., 2015; Virbasius and Czech, 2016; Vitorino et al., 2015). A pathway involving MAP4K4 and proteins with FERM domains was discovered that facilitated focal adhesion disassembly and membrane retraction, promoting cellular movement (Vitorino et al., 2015). This occurred due to the phosphorylation of moesin (a FERM domain-containing protein), and the indirect inhibition of β1-integrin through the removal of talin (another FERM domain-containing protein), an activator of β1-integrin (Vitorino et al., 2015). Consistent with this finding is that MAP4K4 phosphorylates FARP1 and is thus an upstream regulator of FARP1 (Schwaid et al., 2015; Virbasius and Czech, 2016).

As mentioned above, the Rho GTPase specificity for FARP1 seems to be controversial. We know that Rho GTPases have overlapping temporal and spatial activity zones created by Rho GTPase cycling and that Rho, Rac, and Cdc42 gradients exist (Fritz and Pertz, 2016). However, it is unclear how they are affected by FARP1.

Figure 15. Structure of FARP1 domains. Adapted from Kuo et al., 2018.

1.5 The Atypical Rho GTPase RND3

RND3, initially described as RhoE in 1996 (Foster et al., 1996), is an atypical Rho GTPase that is GTPase deficient (Aspenström, 2018; Chardin, 2006; Foster et al., 1996; Riou et al., 2013). The conserved amino acids in Ras family proteins necessary for GTP hydrolysis were identified in tumours caused by Ras signalling that had mutations compromising the hydrolytic activity towards GTP (Foster et al., 1996). From this, RND3 was determined to be constitutively GTP-bound due to amino acid substitutions corresponding to mutated Ras, and therefore RND3 does not switch between active and inactive forms (Aspenström, 2018; Chardin, 2006; Foster et al., 1996; Riou et al., 2013).

RND3 localizes to the cytoplasm, and to the plasma membrane due to positively charged amino acids at its N-terminus which helps with interacting with the negatively charged plasma membrane lipids (**Figure 19b**), (Chardin, 2006; Foster et al., 1996). Lipid modifications at the C-terminus are also necessary for cytoplasmic and plasma membrane localization (Chardin, 2006; Foster et al., 1996).

Since atypical Rho GTPases do not cycle between active and inactive forms like classical Rho GTPases, they are regulated through PTMs and through protein-protein interactions. Most Rho GTPases are geranylgeranylated, and this geranylgeranyl group is recognized by Rho GDIs, which can remove Rho GTPases from the plasma membrane and inactivate them (Foster et al., 1996; Nobes et al., 1998; Riou et al., 2013). However, RND3 is farnesylated due to a methionine in the CAAX motif, so Rho GDIs do not recognize this farnesyl group (Foster et al., 1996; Riou et al., 2013). Instead, RND3 is kept inactive in the cytoplasm by 14-3-3 proteins, which act similarly to Rho GDIs but instead recognize the farnesyl group (Riou et al., 2013). In order for 14-3-3 proteins to interact with RND3, RND3 must first be phosphorylated by ROCKI and protein

kinase C (PKC)α, which then allows 14-3-3 binding (Riou et al., 2013). When active, RND3 is known to affect the actin cytoskeleton, however the mechanisms by which it does so and the effect induced depends on the cell type (Gottesbühren et al., 2013; Guasch et al., 1998; Jie et al., 2016; Nobes et al., 1998; Riento et al., 2003, 2005; Wennerberg et al., 2003).

RND3 is often studied in cancer, however findings remain inconclusive. Depending on the cancer type, RND3 expression levels differ and RND3 can act as a tumor promoter or suppressor (Paysan et al., 2016). For example, in melanoma, RND3 expression is upregulated and encouraged invasion (Klein and Aplin, 2009). One study on human gastric, colorectal, lung, and breast cancer tissues found that RND3 expression was decreased, and that cells transfected with RND3 showed a diminished ability proliferate and invade (Zhu et al., 2014). However, another study found that RND3 expression was actually increased in gastric cancer tissue and promoted invasion, acting as a possible tumor promoter (Feng et al., 2013). RND3 expression in prostate cancer was found to be lower, and seemed to act as a possible tumor suppressor, because when RND3 was overexpressed, cell cycle progression was impeded and apoptosis was encouraged, stopping cancer cells from proliferating further (Bektic et al., 2005).

RND3, its effect on the actin cytoskeleton, and the mechanisms by which such changes are brought about has been studied in individual, non-migrating cells. However, further research needs to be done in order to determine its role in collectively migrating cells.

2. METHODS

2.1 Cell culture

hTERT immortalized HUVEC (HT73), were maintained using Millipore Sigma's EndoGRO-VEGF Complete Culture Media Kit (catalog #SCME002) and hygromycin B gold (InvivoGen, catalog #ant-hg-1) at a working concentration of 50 μg/mL. Cells were passaged using Corning Cell Culture 1X PBS (Fisher Scientific, catalog # MT21040CV) and Corning 0.05% Trypsin (Fisher Scientific, catalog #MT25052CI).

HEK293 cells were maintained using DMEM (Dulbecco's modified eagle medium), (Fisher Scientific, catalog # 11965092) supplemented with 10% FBS (fetal bovine serum). They were passaged using the same PBS and trypsin mentioned above.

HUVECs expressing fluorescence-based reporters, such as our HT73-mCitrine-RND3 cell line, were made by lentiviral transduction of HUVECs, using lentiviral particles produced in HEK293FT cells. HT73-mCitrine-RND3 cells were maintained with EndoGRO media, hygromycin B gold at a working concentration of 50 μg/mL, and G418 (InvivoGen, catalog #ant-gn-1) at a working concentration of 0.5 mg/mL to maintain expression of the mCitrine-RND3 construct.

2.2 siRNA transfection

For siRNA transfection, 96-well plastic bottom plates (Fisher Scientific, catalog #07-200-588) were coated with bovine collagen solution (Cedarlane, catalog #5005-100ML) diluted 1:100 in PBS and incubated at 37°C for 30 minutes. In the meantime, a premix containing 0.25 μL Lipofectamine RNAiMAX (Fisher Scientific, catalog #13778100) and 20 μL of OptiMEM (Fisher Scientific, catalog #31985070) was incubated at room temperature for 5 minutes. siRNAs (Dharmacon, stock concentration 1 μM) were then added to this premix (final siRNA concentration of 20 nM) and incubated at room temperature for 15 minutes. HUVECs, 15 000 cells/well, were resuspended in 80 μL antibiotics-free media. The cell suspension was then centrifuged at 300 x g for 5 mins to form a cell pellet. The supernatant was aspirated and the pellet was resuspended with 80 μL OptiMEM. HUVECs were then added to the transfection mix (reverse transfection). Collagen solution was removed, and cells and transfection mix (100 μL total), were added to the collagen-coated, plastic bottom 96-well plates and incubated at 37°C for 6 hours. After 6 hours, OptiMEM was replaced with full growth media containing antibiotics. Cells were incubated at 37°C and analyzed 3 days later.

2.3 Live cell imaging and cell tracking

Cell nuclei were stained by adding Hoechst 33343 dye (Fisher Scientific, catalog #H3570) to the media (final concentration 1 in 50 000, or 200 ng/mL) and incubated at 37°C for 30 mins. The Hoechst dye and media mixture was then replaced with 100 μL of full growth media supplemented by 20 mM HEPES pH 7.5 (Sigma-Aldrich, catalog #H0887-100ML) and incubated for 1 hour at 37°C prior to imaging. Time-lapse sequences of cells were acquired at 10 minute intervals over 15 timepoints, using an automated widefield fluorescence microscope (ImageXpress XLS, Molecular Devices), a DAPI filter set and a 4X S Fluor 0.20 NA objective. Cells were tracked and their motility was analyzed using MATLAB scripts and plots of cell density, averaged cell velocity, and coordination were generated. Both cell velocity and coordination were determined by tracking every single nucleus in the field of view every 10 minutes and averaged over 15 timepoints for each well and condition. For example, for 15 timepoints every 10 minutes, the velocity and coordination of the cells was determined, giving us 15 velocity and coordination values for every cell in the well. The average of the 15 velocity and coordination values for each cell was taken and then those values obtained were averaged again over every cell to get a single velocity and coordination value representative of that well. Coordination was calculated using the following formula:

$$V(r) = \frac{1}{N}\sum_{i=1}^{N}\left(\frac{1}{n}\sum_{j=1}^{n}\underbrace{\frac{\mathbf{v}_i \cdot \mathbf{v}_j}{|\mathbf{v}_i|\,|\mathbf{v}_j|}}_{\cos(\varphi)}\right)$$

where r is a distance cut-off to determine cell neighbours (100 μm), N is the number of cells migrating at velocity V_i and n is number of neighbours around N migrating at velocities V_j (Hayer et al., 2016). Coordination was based on tracking each individual cell nuclei in the field of view, measuring their velocity (V_i), and then measuring the velocities of the neighbours of that particular

cell within a 100 μm radius (V_j), and then taking the cosine of the angles between cells and all their neighbours (Hayer et al., 2016). Coordination values were between 0 and 1, where cos (0°) = 1 for cells moving in the same direction, cos (180°) = -1 for cells are moving in opposite directions, and cos (90°) = 0, for cells moving in perpendicular directions (Hayer et al., 2016).

2.4 Real-time quantitative PCR (RT-qPCR)

RT-qPCR was used to assess the knockdown efficiency of siRNA pools and of individual siRNAs on FARP1 and RND3 mRNA levels in HUVEC. This protocol was modified from Croisé et al., 2016. RT-qPCR was done using the $2^{-\Delta\Delta Cq}$ method (Livak and Schmittgen, 2001). Glyceraldehyde-3-phosphate dehydrogenase (GAPDH) was used as a reference/housekeeping gene. For each primer set for both FARP1 and RND3, C_q values between duplicate conditions were averaged and normalized to the average C_q of both GAPDH primers. The following formulas were used to calculate the fold change:

$$\Delta C_q = (\text{average } C_q \text{ of gene of interest, primer set}) - (\text{average } C_q \text{ GAPDH})$$

$$\Delta\Delta C_q = (\Delta C_q \text{ gene of interest, primer set}) - (\Delta C_q \text{ siNT})$$

$$\text{Fold change} = 2^{-\Delta\Delta Cq}$$

The siRNA transfections were scaled up to a 6-well plate format (Fisher Scientific, catalog # 07-200-83). Total RNA from HUVECs transfected with 4 individual siRNAs, and each of these 4 siRNAs pooled, targeting either FARP1 or RND3, was extracted using either Epoch Life Science GenCatch Total RNA extraction kit (Cedarlane, catalog # 1660050) or Qiagen RNeasy Mini Kit (Qiagen, catalog # 74104). An on-column RNase-free DNase I treatment (Qiagen, catalog # 79254) was done using both of these kits to ensure genomic DNA removal. RNA concentration was measured by spectrophotometry and cDNA was made with 1 μg of total RNA and reverse transcriptase (Fisher Scientific, catalog # FEREP0042) for a total reaction volume of 20 μL. The reverse transcription thermal cycling protocol was 60 minutes at 42°C, then 70°C for 10 minutes. RT-qPCR was done with a Bio-Rad PCR machine in 96-well skirted plates (Bio-Rad, catalog # HSP9601), using cDNA diluted 1:20, two different sets of primers (refer to **Table 1**), each specific to our genes of interest, and SYBR green (Bio-Rad, catalog # 1725121) for a total reaction volume

of 10 μL. The RT-qPCR thermal cycling conditions used were 95°C for 30 seconds, 95°C for 10 seconds, and 60°C for 30 seconds, for 40 cycles.

Table 1. Primer sequences used for each gene in RT-qPCR. All primer sequences for primer set #1 were obtained from the Harvard Primer Bank. GAPDH primer set #2 was obtained from Croisé et al., 2016. FARP1 primer set #2 was obtained from Croisé et al., 2016. RND3 primer set #2 was obtained from Bektic et al., 2005. F means forward primer, R means reverse primer.

Gene		**Primer Sequences**	
		Primer set #1 (5' → 3')	**Primer set #2 (5' → 3')**
GAPDH	F	CTGGGCTACACTGAGCACC	TGCACCACCAACTGCTTAGC
	R	AAGTGGTCGTTGAGGGCAATG	GGCATGGACTGTGGTCATGAG
FARP1	F	ATTCGGGGATCAGTACCTTGG	GCACAGCTCCACGGTACGAT
	R	ATGGACACGAGTTTTCCTGAAG	ACGGATGAACTCCCTTCCCG
RND3	F	TTACACGGCCAGTTTTGAAATCG	ACTGCGCTGCTCCATGTCT
	R	GGGCGGACATTGTCATAGTAAG	TCGATTTCAAAACTGGCCGT

2.5 siRNA-resistant rescue construct

RND3 cDNA was obtained from a clone provided to us by the Goodman Cancer Center (clone #: O-795-1, clone ID: DQ890666). A pLV-mCitrine-RND3-IRES-NEO construct was generated first by digesting a pLV-mCitrine-PXN-IRES-NEO plasmid using BsrGI (New England Biolabs, catalog # R3575S) and EcoRI (New England Biolabs, catalog # R3101S) restriction enzymes to generate a vector backbone for N-terminal in-frame fusion to mCitrine. The digest took place at 37°C for 1 hour. A synonymous mutation spanning the region where siRND3#2 binds was generated based on codon degeneracy (siRND3#2 binding site: UAGUAGAGCUCUCCAAUCA, siRND3#2 binding site with synonymous mutation: CTGGTGGAGCTGAGCAATCAC). We used a database called High-performance Integrated Virtual Environment-Codon Usage Tables (HIVE-CUTs), (Athey et al., 2017) to determine the codon usage for different amino acids.

Two RND3 PCR reactions were done in order to generate two overlapping portions of RND3 bearing the mutated region. Subsequently, the two PCR products were inserted into the digested vector backbone using Gibson assembly. Primer sequences are listed in **Table 2**. Generation of an siRNA-resistant rescue construct was also attempted to be made for FARP1, however PCR amplification of FARP1 from a cDNA library was unsuccessful. The primer sequences used for FARP1 are also listed in **Table 2**.

Table 2. Primer sequences for the PCR amplification of FARP1 and RND3 and for the generation of an siRNA-resistant rescue construct for RND3. F means forward primer, R means reverse primer.

Gene		Primer sequences (5' → 3')
FARP1	F	CTCGGCATGGACGAGCTGTACAAGAGTGCTGGTGGTAGTGGAGAAATAGAGCAGAGGCCG
	R	GACTCTAGAGCGGCCGCCCTCGAGGAATTCTCAATACACAAGAGACTCTTTGTGACTC
RND3	F	CTCTCGGCATGGACGAGCTGTACAAGAGTGCTGGTGGTAGTAAGGAGAGAAGAGCCAGCC
	R	GACTCTAGAGCGGCCGCCCTCGAGGAATTCTCACATCACAGTGCAGCTCTTC
	Primer sequences for RND3 siRNA-resistant rescue construct (5' → 3')	
	F	ACACTGGTGGAGCTGAGCAACCATAGGCAGACGCCAGTGTCC
	R	CCTATGGTTGCTCAGCTCCACCAGTGTACTAACATCTGTCCGCAGATCAGAC

2.6 Fixed Cell Imaging (Immunofluorescence)

96-well glass-bottom plates were coated with bovine collagen solution diluted 1:100 in PBS and incubated at 37°C overnight (16-24 hours). The next day, HUVECs (5000 cells/well – 15 000 cells/well, depending on the experiment) were transfected with siRNAs as described above. On the third day, cells were fixed with a fixation solution made of 4% paraformaldehyde (Fisher Scientific, catalog # 50-980-487) in PBS and added at a 1:1 ratio to culture medium so that the final concentration of paraformaldehyde was 2%. The fixation solution was kept on cells for 15 minutes at room temperature, and then removed. Cells were then washed with PBS and then incubated with permeabilization/blocking solution (0.1% Triton X-100, 10% FBS, 1% BSA, 0.01% NaN_3, in PBS) for 30 minutes at room temperature. Rabbit anti Phospho-Myosin Light Chain 2 (Cell Signaling Technology, catalog # 3674S) was used as a primary antibody diluted 1:200 in permeabilization/blocking solution. Cells were incubated with the primary antibody either at room temperature for 2 hours, or overnight at 4°C, and then rinsed three times with PBS. Cells were then stained with Alexa Fluor 647 goat anti-rabbit secondary antibody (Fisher Scientific, catalog # A21244) diluted 1:1000 in permeabilization/blocking solution, and Alexa Fluor 555 phalloidin (New England Biolabs, catalog #8953S) diluted 1:200 in permeabilization/blocking solution for 1 hour at room temperature. Cells were rinsed with PBS three more times, and if nuclei were not previously stained with Hoechst dye (final concentration 1 in 50 000, or 200 ng/mL), it was added in the second wash, incubated at room temperature for 10 minutes, and then removed.

Cells were then imaged with a Nikon Ti2 widefield fluorescence microscope and a Nikon 20X 0.75 NA objective.

To quantify mean F-actin and phospho-myosin light chain (pMLC) content in immunostained HUVEC, we used a MATLAB script that performed single cell measurements of

cells in images of cell monolayers. Cell nuclei stained with Hoechst dye were detected and expanded by 24 pixels to generate a ring around them, and background-subtracted signals of phalloidin and pMLC were measured.

3. RESULTS

3.1 Rho GEF and Rho GTPase expression analysis

We first wanted to determine if the possible candidate regulators of collective cell migration (FARP1 and RND3) determined from the siRNA screen were expressed in endothelial cells. Using The Human Protein Atlas Database (Uhlén et al., 2015), we downloaded an RNA-Seq dataset of 64 human cell lines. We then used MATLAB scripts to generate a plot of all Rho GEFs and all Rho GTPases and their corresponding expression in three endothelial cell lines (**Figure 16**), relative to all other cell lines in the dataset. Of the 64 cell lines within the dataset (gray dots), the three endothelial cell lines were HUVEC TERT2 (green dots), TIME (red dots), and hTEC/SVTERT24-B (blue dots). Since we were using HUVECs in our research, we wanted to make sure that our two candidate regulators were indeed expressed, and to what extent compared to other endothelial cell lines.

The Rho GEFs (**Figure 16a**) and Rho GTPases (**Figure 16b**) were sorted based on their averaged expression levels in the three endothelial cell lines. HUVEC TERT2 and TIME had similar relative gene expression profiles, with hTEC/SVTERT24-B being more divergent. In addition, it seems like for these endothelial cell lines, Rho GEFs and Rho GTPases are not highly expressed as compared to the other cell lines, with some of the other cell lines having much higher TPMs than our three endothelial ones, however this is more evident in the plot with Rho GEFs (**Figure 16a**).

Considering that both FARP1 and RND3 are located in the upper half of the ranked lists, this suggests that their expression is above average compared to other Rho GEFs and Rho GTPases in endothelial cells. We therefore conclude that both FARP1 and RND3 are expressed in endothelial cell types.

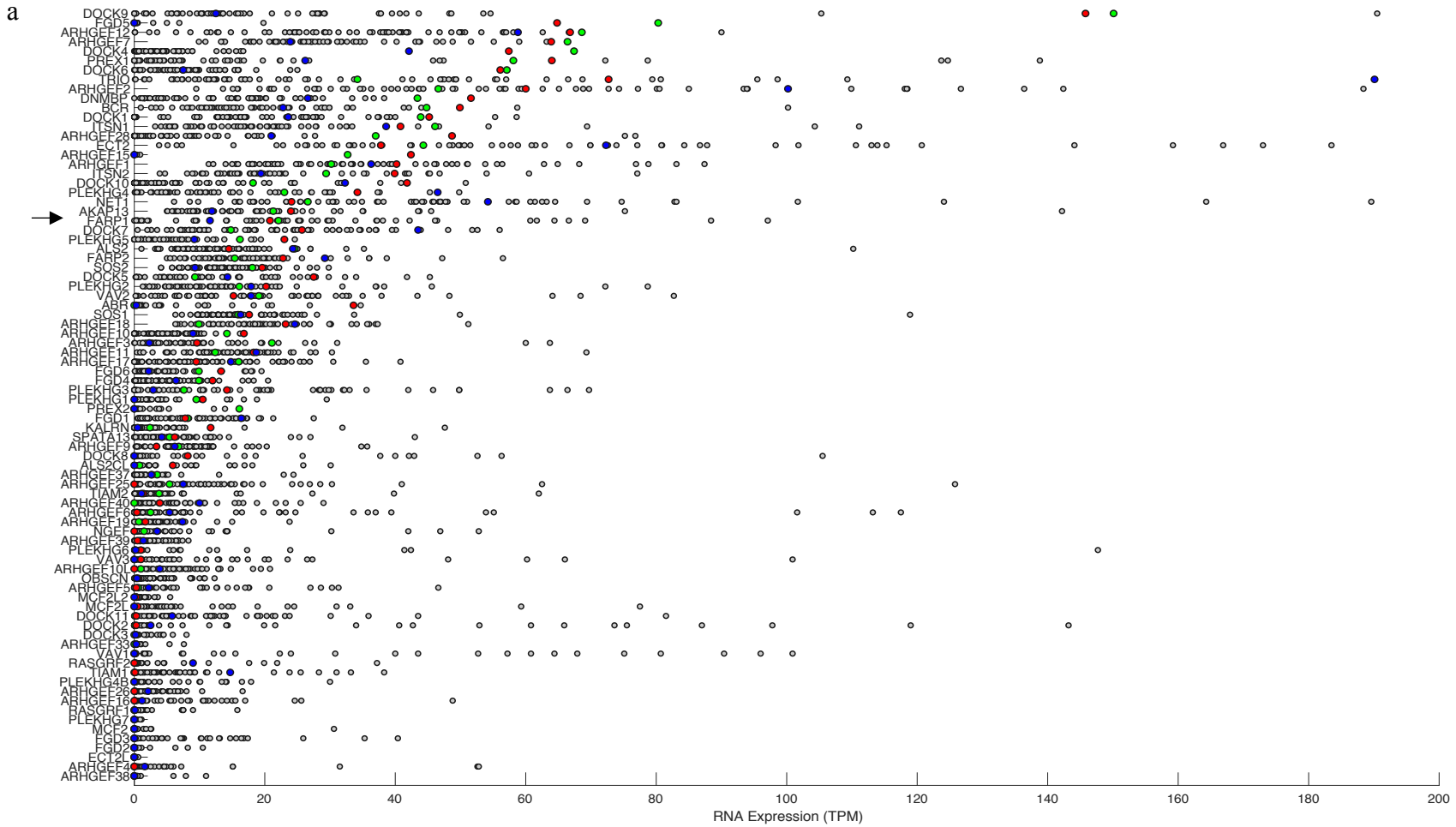
a
DOCK9
FGD5
ARHGEF12
ARHGEF7
DOCK4
PREX1
DOCK6
TRIO
ARHGEF2
DNMBP
BCR
DOCK1
ITSN1
ARHGEF28
ECT2
ARHGEF15
ARHGEF1
ITSN2
DOCK10
PLEKHG4
NET1
AKAP13
FARP1
DOCK7
PLEKHG5
ALS2
FARP2
SOS2
DOCK5
PLEKHG2
VAV2
ABR
SOS1
ARHGEF18
ARHGEF10
ARHGEF3
ARHGEF11
ARHGEF17
FGD6
FGD4
PLEKHG3
PLEKHG1
PREX2
FGD1
KALRN
SPATA13
ARHGEF9
DOCK8
ALS2CL
ARHGEF37
ARHGEF25
TIAM2
ARHGEF40
ARHGEF6
ARHGEF19
NGEF
ARHGEF39
PLEKHG6
VAV3
ARHGEF10L
OBSCN
ARHGEF5
MCF2L2
MCF2L
DOCK11
DOCK2
DOCK3
ARHGEF33
VAV1
RASGRF2
TIAM1
PLEKHG4B
ARHGEF26
ARHGEF16
RASGRF1
PLEKHG7
MCF2
FGD3
FGD2
ECT2L
ARHGEF4
ARHGEF38
0
20
40
60
80
100
120
140
160
180
200
RNA Expression (TPM)

b

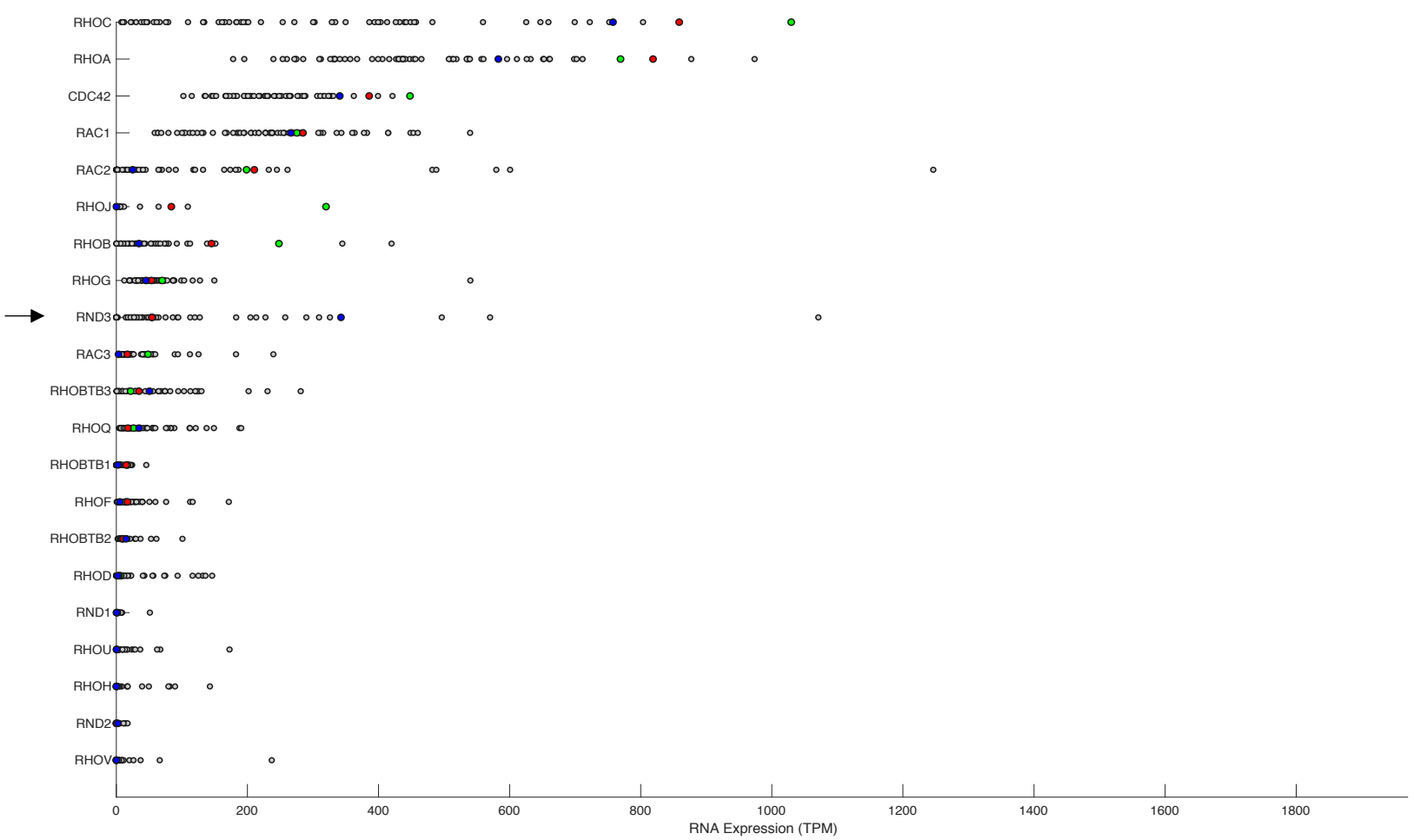

Figure 16. Expression analysis in three endothelial cell lines. Green dots represent the HUVEC TERT2 cell line, red dots represent the TIME cell line, and blue dots represent the hTEC/SVTERT24-B cell line. TPM refers to transcripts per million. Gray dots are other cell lines. **(a)** Expression analysis of Rho GEFs in three cell lines **(b)** Expression analysis of Rho GTPases in three cell lines.

3.2 Optimization of the siRNA transfection protocol

One of the major challenges encountered in this project was getting the siRNA transfection protocol to work. For a while, control siRNAs did not produce the expected cellular phenotype, i.e. cell cycle arrest/cell death upon transfection of siKIF11, which targets a mitotic kinesin. Other issues encountered were uneven cell monolayers, incorrect siRNA concentrations due to errors by the manufacturer, and lack of reproducibility of weak phenotypes. Finally, after extensive troubleshooting, we found that there must be an unidentified component in the endothelial growth media, which interfered with the siRNA transfection. This was determined by validating all components involved in the transfection (transfection reagents, siRNAs, culture media, and serum-reduced transfection media) in both HUVEC and HEK293 cells, using our positive control, siKIF11, for transfection. We adjusted the protocol such that prior to transfection, we pelleted the cells and resuspended them before plating in reduced serum media (OptiMEM) instead of full growth media. OptiMEM was then replaced with full growth media after a 6-hour incubation period.

3.3 Validation of siRNA screening candidates FARP1 and RND3 using siRNA pool deconvolution

Using pools of four siRNAs (siRNA#1 + siRNA#2 + siRNA#3 + siRND#4) targeting different regions of each gene, we attempted to verify the phenotypes previously identified in the siRNA screen for both FARP1 and RND3. siRNA pools were used because siRNAs are known to have off-target effects, and using pools minimizes the probability of this by "diluting" out off-target effects (Hannus et al., 2014). Nevertheless, off-target effects of individual siRNAs in the pool might dominate the phenotype. siRNA pool deconvolution, where each of the individual siRNAs from the pool (siRNA#1, siRNA#2, siRNA#3, siRNA#4) and the pool are separately transfected into cells, can then be used to further assess possible off-target effects.

The purpose of this experiment was to validate FARP1 and RND3 as candidate regulators, and to determine which individual siRNAs from the pools of 4 produced the observed phenotypes. From this, we would determine whether there was a correlation between knockdown efficiency and migration phenotype, as well as knockdown specificity by making an siRNA-resistant rescue construct.

The negative control used was a non-targeting siRNA (siNT) which was designed to not target any gene in the human genome and therefore should not have any effect on the cell's density or motility parameters. siKIF11 was our positive control for transfection. KIF11 is a kinesin necessary for proper chromosome segregation. When KIF11 is knocked down, cells cannot divide properly, resulting in decreased cell number. This transfection control enabled us to rapidly verify whether cells had taken up the siRNAs by monitoring cell density.

HUVECs were transfected with a pool of 4 siRNAs that target different regions of each gene, and each one of these siRNAs individually. Cell nuclei were stained with Hoechst dye and then tracked using an automated widefield fluorescence microscope. Images were acquired at 10

minute intervals for 2.5 hours. Using MATLAB scripts, plots of cell density, velocity, and coordination were generated.

The reason cell density was monitored was to ensure that the transfection was working and that the cells were taking up the siRNAs. Two types of siKIF11 were used; siKIF11(pool) was ordered from a company (Dharmacon), and siKIF11(Y) was made by my supervisor (**Figure 17a**). When cells are transfected with siKIF11, an approximately 50% decrease in cell density compared to siNT is expected, which is why the cell densities for both siKIF11 are low (**Figure 17a**). This indicated that the transfection worked well and that cells had taken up the siRNAs. The cell density for the rest of the siRNA conditions (siFARP1#1-4, siFARP1(pool) and siRND3#1-4, siRND3(pool)) were all between approximately 350-600 cells/mm^2 and well above the cell densities produced by siKIF11, indicating that these siRNAs were not toxic to the cells or induced cell death (**Figure 17a**). Lastly, nontransfected cells have the highest cell density because they are not siRNA-transfected. This is expected, as siRNA transfection reagents generally affect cell health (**Figure 17a**).

From all the FARP1 siRNAs, siFARP1#3 showed a decrease in both coordination and velocity (**Figure 17b**, **c**). From all the RND3 siRNAs, it was siRND3#2 that showed the strongest increase in coordination and decrease in velocity (**Figure 17b**, **c**). siRND3(pool) also showed a coordination increase, although it was slightly lower than siRND3#2 but higher relative to siNT (**Figure 17b**). We noticed significant variability between biological replicates in the velocity and coordination figures. This could be due to not all cells within a well taking up the siRNAs efficiently, or due to different passage numbers of the cells used to do each biological replicate (i.e. some plates were at passage 3 for one replicate, others at passage 5, etc.). Based on this,

perhaps a larger number of cells can take up siRNAs when they are newer versus when cells are older, which is a potential cause of variability between biological replicates.

From these results, siFARP1#3 and siRND3#2 were the siRNAs that produced similar phenotypes to those seen in the screen. Although we have determined a phenotypic match, this does not yet confirm the data from the original screen, as the phenotypes observed for siFARP1#3 and siRND3#2 in our validation assay could still be due to off-target effects. With these phenotypes, we proceeded to determine how they are related to knockdown efficiencies using RT-qPCR. We would then use these siRNA sequences to create an siRNA-resistant rescue construct, which will determine knockdown specificity and conclusively determine whether FARP1 and RND3 are regulators of collective endothelial cell migration.

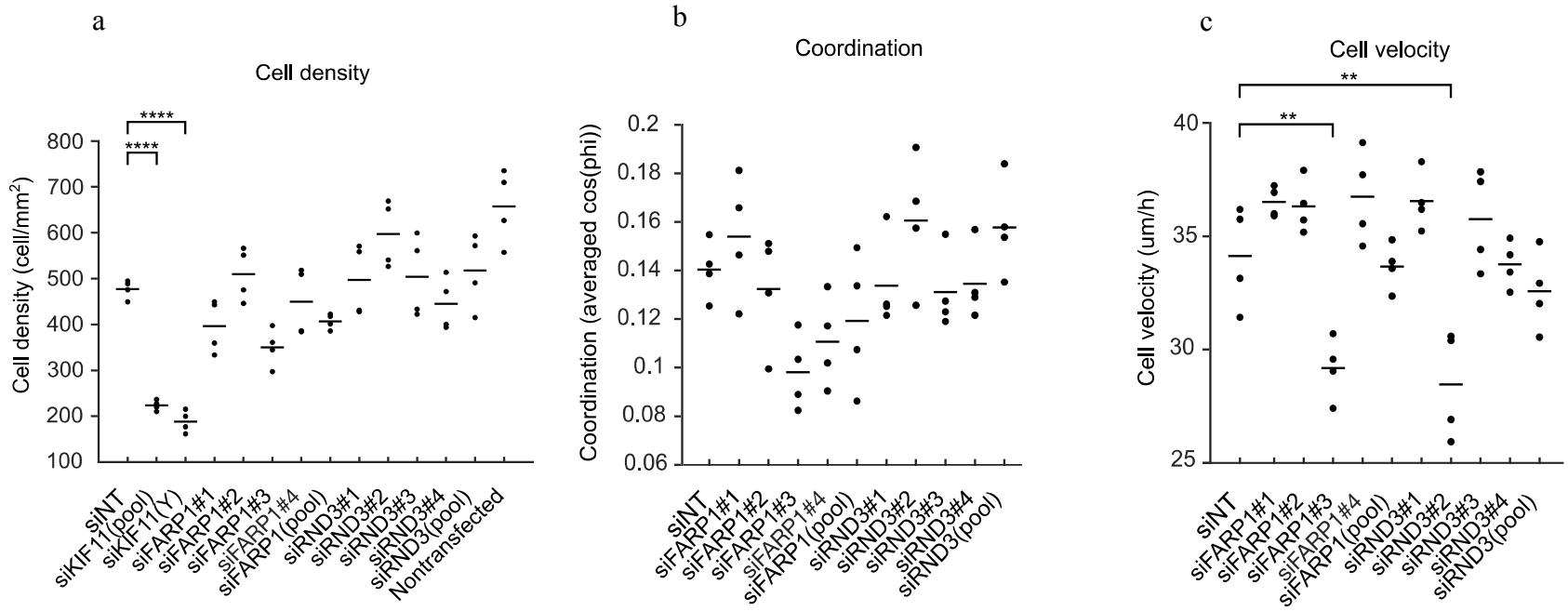

Figure 17. siRNA validation assay- siFARP1#3 and siRND3#2 show similar migration phenotypes to those seen in the original screen. Plots of **(a)** cell density (cells/mm^2), **(b)** coordination and **(c)** cell velocity (μm/hour) in HUVEC monolayers transfected with siRNAs. Each siRNA condition was done in duplicate (technical replicates) and averaged. Each data point represents a biological replicate (n = 4). Cell motility data from 15 timepoints was taken by averaging values obtained every 10 minutes for 2.5 hours of a time-lapse sequence. Due to focus drift, only data from timepoints 6 to 15 was taken. The horizontal line between the data points in each condition represents the mean of those data points in that condition. Statistical analysis was done using an ordinary one-way ANOVA followed by Tukey's multiple comparisons test. ****P < 0.0001 (cell density), **P = 0.0076 (cell velocity, siNT vs. siFARP1#3), **P = 0.014 (cell velocity, siNT vs. siRND3#2). Coordination values are not significant.

3.4 siRND3#2 and siRND3(pool) strongly reduce mRNA levels

To further validate the siRNA screen results, we tested the knockdown efficiency of the individual siRNAs by measuring the mRNA levels of siRNA-transfected cells. The purpose was to determine if the knockdown of individual siRNAs was correlated with the migration phenotypes. If this was not the case, it implied an off-target effect and that the observed phenotypes are not due to reduced FARP1 and RND3 expression.

This was done using RT-qPCR. HUVECs were transfected with siRNAs, and then RNA was extracted from them. cDNA was then generated using reverse transcriptase and the resulting cDNA was used as a template in the RT-qPCR reactions. Two primer pairs were used for each gene, SYBR green was used as a fluorescent dye, and GAPDH was used as a reference gene.

siRND3#2 and siRND3(pool) both showed a strong decrease in mRNA levels with only about 10% of mRNA remaining for both sets of primers relative to siNT (**Figure 18a**). They also showed the strongest effect on coordinated cell movement (**Figure 17b**). siRND3#4 also knocked down RND3 mRNA though to a lesser degree (15% mRNA remaining relative to siNT), (**Figure 18a**), and with no effect on cell migration parameters (**Figure 17b**, **c**). From this, we concluded that of the four individual siRNAs, siRND3#2 was most efficient in knocking down RND3 mRNA, and likely responsible for producing the migration phenotype. To further test whether the effect of siRND3#2 on cell migration was not due to an off-target effect, we designed a rescue construct that was resistant to siRND3#2. Expression of siRNA-resistant RND3 in siRND3#2 treated cells should then rescue the migration behaviour to control-treated cells. This siRNA-resistant rescue construct was made with synonymous mutations in the region targeted by siRND3#2.

For FARP1, of the four individual siRNAs, siFARP1#3 showed the strongest effect on cell migration parameters and hence this was expected to be due to the most efficient mRNA

knockdown. However, this was not the case. Instead, siFARP1#1, siFARP1#4, and siFARP1(pool) all showed stronger reductions in mRNA levels compared to siFARP1#3 (**Figure 18b**). siFARP1#2 neither knocked down FARP1 expression nor caused significant changes in migration behaviour (**Figure 18b**). A possible explanation for these results are off-target effects. Due to time limitations, we decided to not further pursue FARP1 as a candidate regulator and instead focus on further investigating the role of RND3 in regulating collective cell migration.

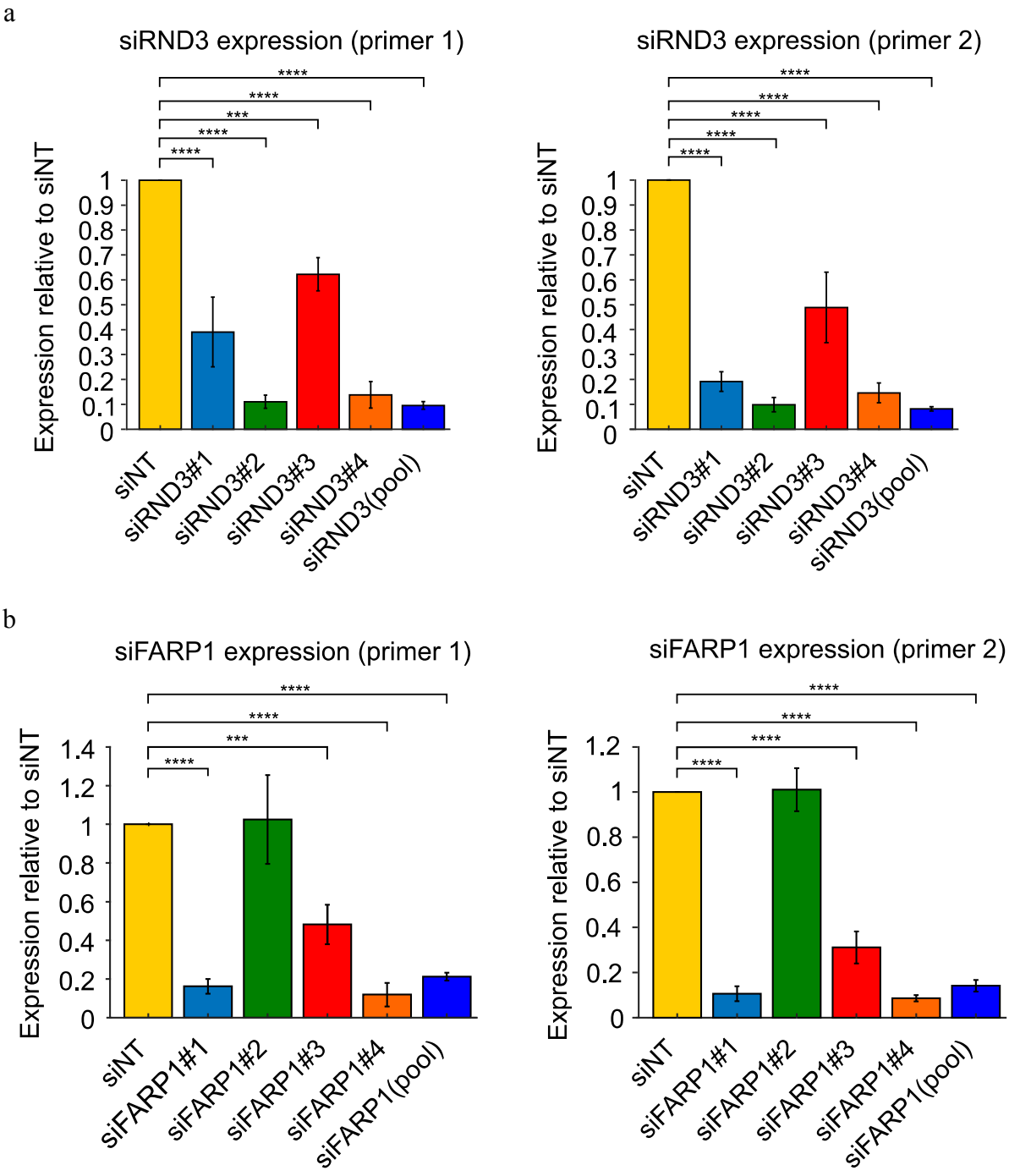

Figure 18. Relative fold change of mRNA levels of RND3 **(a)** and FARP1 **(b)** in HUVECs using siRNA pool deconvolution. The expression of FARP1 and RND3 was normalized to GAPDH expression. The graphs represent the average fold change relative to siNT (control condition) from three independent experiments. Two primer pairs specific for FARP1, RND3, and GAPDH were used. Statistical analysis was done using an ordinary one-way ANOVA followed by Tukey's multiple comparisons test. ****P < 0.0001, ***P = 0.0002 (siNT vs. siRND3#3, primer 1), ***P = 0.0007 (siNT vs. siFARP1#3, primer 1).

3.5 Creating an siRNA-resistant rescue construct

To determine knockdown specificity, we created an siRNA-resistant rescue construct with synonymous mutations in the region where siRND3#2 binds (**Figure 19a**). With this, siRND3#2 would not be able to knock down the resulting mRNA, while encoding the identical protein. We generated a cell line overexpressing this synonymous mutation (**Figure 19b**), knocked down RND3 using siRND3#2, and compared the migration phenotypes with parental HUVEC (HT73) to see if they were rescued.

To amplify the newly mutated region as well as the portions flanking it, we performed two PCR reactions and assembled the construct together by Gibson assembly. The construct was introduced to HUVECs via lentiviral transduction, resulting in a cell line stably expressing mCitrine-RND3 (HT73-mCitrine-RND3).

To validate our approach, we first transfected siNT, siRND3#2, and siRND3(pool) into HT73-mCitrine-RND3, in which exogenously expressed RND3 levels can be monitored due to mCitrine fluorescence (**Figure 19b**). As expected, siNT and siRND3#2 did not reduce mCitrine-RND3 levels, whereas siRND3(pool) almost completely eliminated mCitrine-RND3 expression. This confirmed that (1) our rescue construct was resistant to siRND3#2 as expected and (2) that our rescue construct was effectively eliminated by the remaining siRNA in the pool.

In addition to knockdown/rescue experiments, this HT73-mCitrine-RND3 cell line will be used to assess the effect of RND3 overexpression on cell motility and on actin cytoskeletal organization.

a

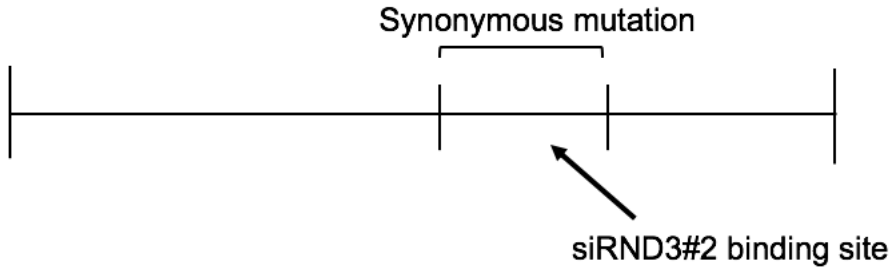

b

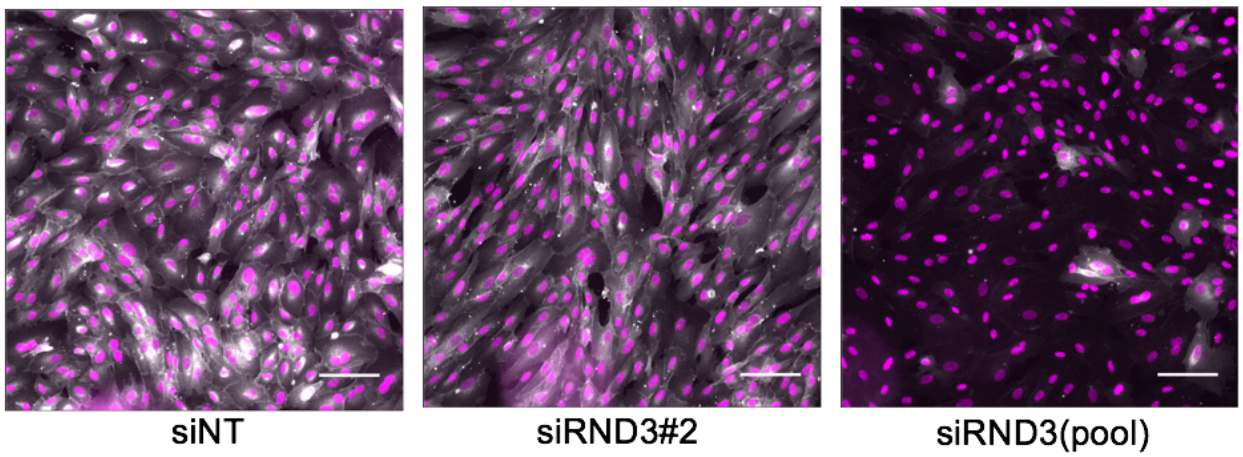

Figure 19. Creation of an siRNA-resistant rescue construct and its introduction into HUVECs. **(a)** Schematic of how the siRNA-resistant rescue construct was created **(b)** Fluorescence microscopy images of the mCitrine-RND3 channel (grayscale) and nuclei (magenta) stained with Hoechst dye. Scale bars are 100 μm. As expected, siRND3(pool) but not siRND3#2 depleted siRND3#2-resistant mCitrine-RND3 from cells.

3.6 Expression of siRNA-resistant mCitrine-RND3 does not rescue the migration phenotype of RND3 depletion

To determine if the migration phenotype (decrease in velocity, increase in coordination) obtained with siRND3#2 was rescued by the expression of siRND3#2-resistant mCitrine-RND3, we performed the same siRNA assay described above, except with two cell lines: parental HUVEC (HT73), and HUVEC overexpressing the siRNA-resistant rescue construct (HT73-mCitrine-RND3). Both cell lines were transfected with siNT, siRND3#2, and siRND3(pool). siKIF11 was used as a transfection control. Cells were tracked and MATLAB scripts were used to plot cell density, velocity, and coordination. **Table 3** provides an overview of the effect on RND3 expression according to the siRNA each cell line was transfected with.

Table 3. Overview of the anticipated effects on RND3 expression in HT73 and HT73-mCitrine-RND3 cells transfected with different siRNAs. Exogenous refers to the construct resistant to siRND3#2.

Cell line	siRNA	Effect on RND3	Explanation
HT73	siNT	No effect (baseline expression)	siNT does not knock down any genes
	siRND3#2	Knockdown	Knockdown of endogenous RND3
	siRND3(pool)	Knockdown	siRND3(pool) has all 4 siRNAs → RND3 is knocked down
HT73-mCitrine-RND3	siNT	Overexpression	Both endogenous and exogenous RND3 present
	siRND3#2	Overexpression	Knocking down only endogenous RND3, exogenous still present
	siRND3(pool)	Knockdown	siRND3#2 knocks down endogenous, siRND3#1, 3, 4 knock down exogenous

Plotting the resulting cell density for all conditions showed a strong reduction in cell number in the presence of siKIF11, confirming efficient siRNA transfection into both cell types (**Figure 20a**). The goal of this experiment was to determine knockdown specificity. If the phenotype seen with siRND3#2 in the validation assay is rescued, this would rule out any off-

target effects. For both coordination and velocity, we expected the phenotypes observed with siRND3#2 from the knockdown validation assay (decrease in velocity, increase in coordination) to be rescued, such that the values were similar to those seen in the non-targeting condition in HT73 cells. However, this was not the case. The coordination values for cells with the mCitrine-RND3 construct all had similar values, although they were slightly lower than those seen in HT73 cells (**Figure 20b**). For cell velocity, overexpression did not rescue the phenotypes seen with RND3 knockdown, although values were slightly higher than those with RND3 knockdown in HT73 cells (**Figure 20c**).

Lastly, the coordination values in this siRNA rescue assay (**Figure 20b**) were much lower than those in the siRNA validation assay (**Figure 17b**). The exact same protocol was followed for both these experiments. The only difference was that the validation assay was done using plastic 96-well plates whereas the rescue assay was done using glass 96-well plates, and perhaps this could have affected cell coordination (further discussed in the Discussion).

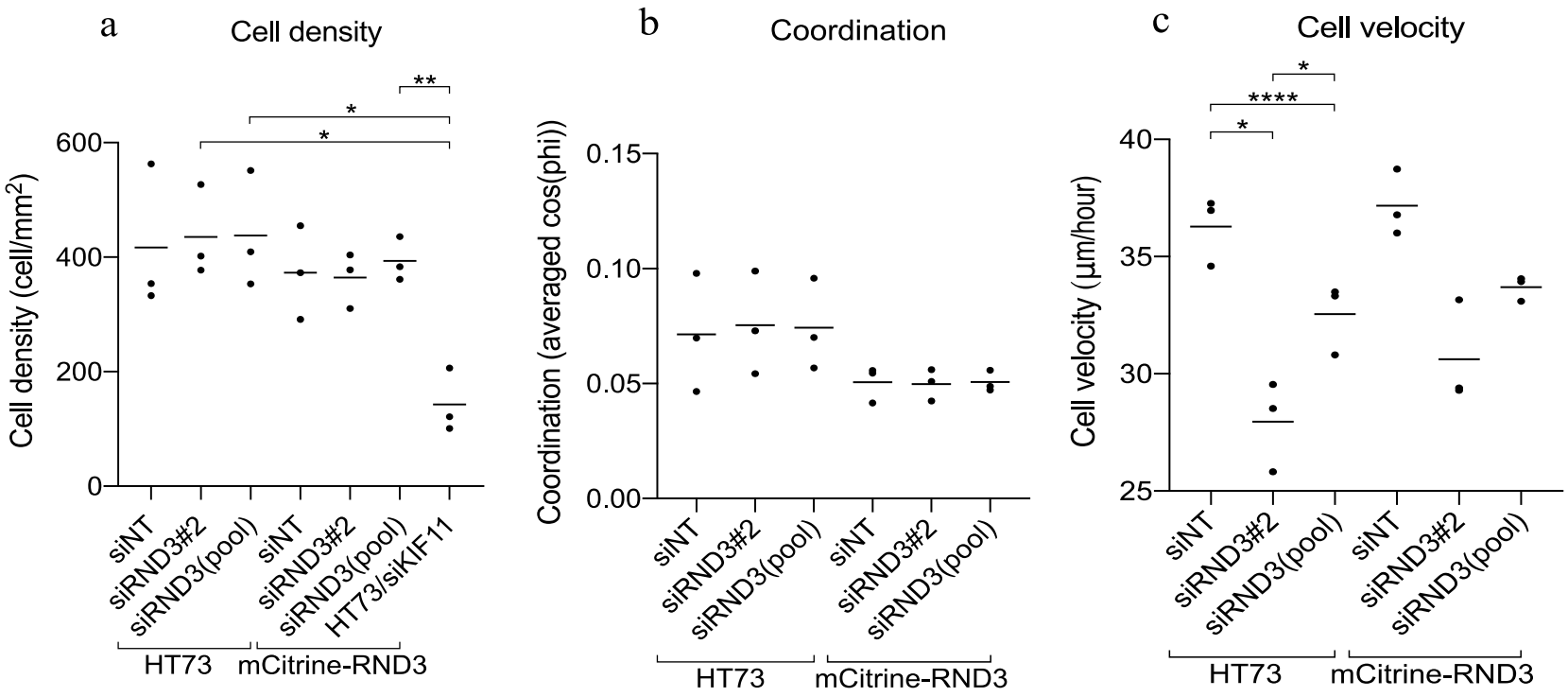

Figure 20. siRNA rescue assay. Plots of **(a)** cell density (cells/mm^2), **(b)** coordination and **(c)** cell velocity (µm/hour) in HUVEC monolayers transfected with siRNAs. Each siRNA condition was done in triplicate (technical replicates) and averaged. Each data point represents a biological replicate (n = 3). Cell motility data from 15 timepoints was taken by averaging values obtained every 10 minutes for 2.5 hours of a time-lapse sequence. Due to focus drift, only data from timepoints 6 to 15 was taken. The horizontal line between the data points in each condition represents the mean of those data points in that condition. A repeated measures one-way ANOVA followed by Tukey's multiple comparisons test was performed. *P = 0.0167 (cell density, HT73/siRND3#2 vs. HT73/siKIF11), **P = 0.0081 (cell density, mCitrine-RND3/siRND3(pool) vs. HT73/siKIF11), *P = 0.0328 (cell density, HT73/siRND3(pool) vs. HT73/siKIF11) , *P = 0.0109 (cell velocity, HT73/siNT vs. HT73/siRND3#2), ****P < 0.0001 (cell velocity, HT73/siNT vs. HT73/siRND3(pool)), *P = 0.0269 (cell velocity, HT73/siRND3#2 vs. HT73/siKIF11). Coordination values are not significant.

3.7 RND3 depletion and overexpression both increase F-actin and myosin activity in HUVECs

Subsequent to cell tracking, we performed immunofluorescence staining to determine whether RND3 depletion and overexpression had detectable effects on actin and myosin cytoskeletal organization. Cells were fixed with paraformaldehyde, and stained with pMLC antibody to visualize myosin-II, and fluorescently-tagged phalloidin to visualize F-actin. Images were captured using a widefield fluorescence microscope, and analyzed using a MATLAB script. The MATLAB script detected cell nuclei based on Hoechst 33343 signal, nuclei were dilated (24 pixels) to generate cytoplasmic rings, wherein background-subtracted pMLC and phalloidin signals were measured and averaged over thousands of cells per condition.

The non-targeting condition in HT73 cells represents baseline levels of F-actin and myosin activity (**Figure 21**, **Figure 22**). When RND3 was depleted in HT73, we observed an increase in F-actin content compared to the non-targeting condition for both siRND3#2 and siRND3(pool), however this increase was stronger, both qualitatively and quantitatively, with siRND3#2 (**Figure 21a**, **b**). Myosin activity remained unchanged (**Figure 22a**, **b**).

In cells overexpressing mCitrine-RND3, both F-actin and myosin activity were higher than in parental HUVEC (**Figure 21**, **Figure 22**). Surprisingly, siRNA depletion of RND3 in these cells increased F-actin content further, with the strongest effect observed with siRND3#2 (**Figure 21a**, **b**). Thus, both RND3 depletion and RND3 overexpression increased F-actin in cells.

Lastly, we made the intriguing observation that siRND3-treated cells were more elongated and organized in streams compared to control cells, suggesting a role of RND3 in determining cell shape and/or cell-cell interaction (**Figure 23**).

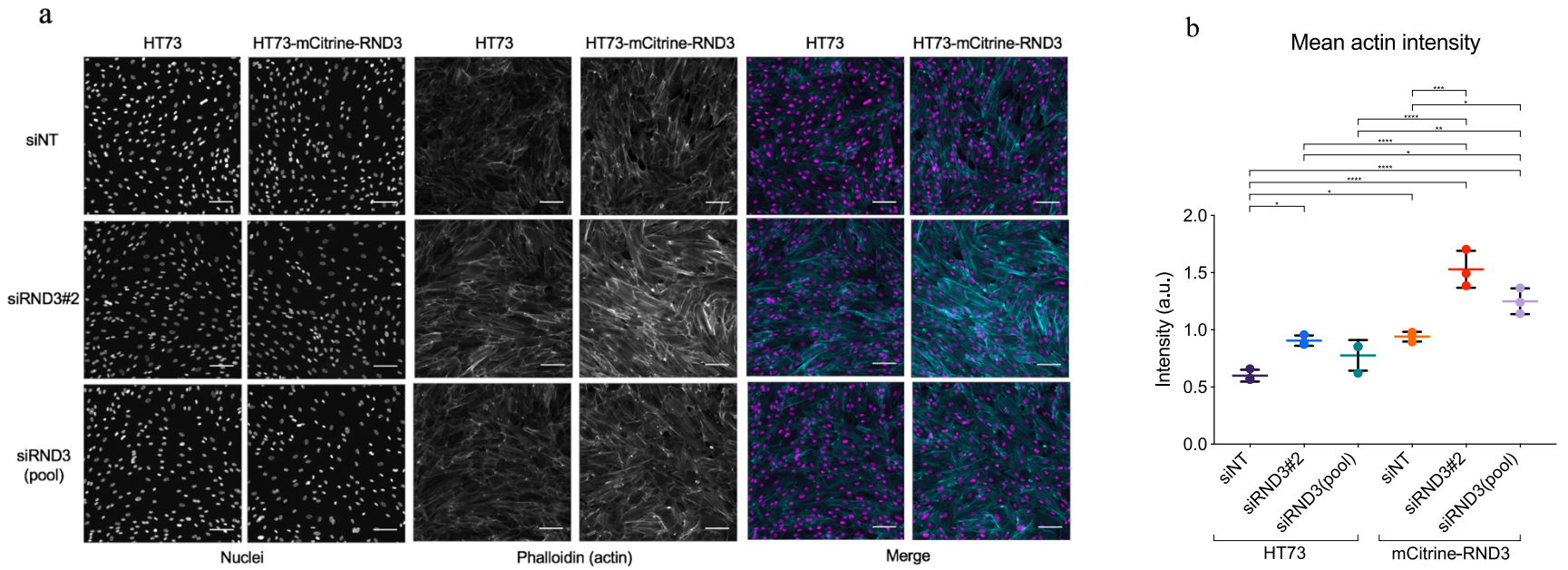

Figure 21. Effect of RND3 depletion and overexpression on the actin cytoskeleton in parental HUVEC (HT73) and HUVEC containing the mCitrine-RND3 construct (HT73-mCitrine-RND3). Each data point represents a biological replicate (n = 3). **(a)** Immunofluorescence images of F-actin, labelled with phalloidin 555. Scale bars for all images are 100 µm. **(b)** Quantification of mean fluorescence intensity of actin, measured in cytoplasmic rings surrounding the cell nuclei. Actin fluorescence intensities were normalized and an ordinary one-way ANOVA and Tukey's multiple comparisons test was performed. *P = 0.0309 (HT73/siNT vs. HT73/siRND3#2), *P = 0.0155 (HT73/siNT vs. mCit-RND3/siNT), ****P < 0.0001 (HT73/siNT vs. mCit-RND3/siRND3#2), ****P < 0.0001 (HT73/siNT vs. mCit-RND3/siRND3(pool)), ****P < 0.0001 (HT73/siRND3#2 vs. mCit-RND3/siRND3#2), *P = 0.0145 (HT73/siRND3#2 vs. mCit-RND3/siRND3(pool)), ****P < 0.0001 (HT73/siRND3(pool) vs. mCit-RND3/siRND3#2), **P = 0.0012 (HT73/siRND3(pool) vs. mCit-RND3/siRND3(pool)), ***P = 0.0002 (mCit-RND3/siNT vs. mCit-RND3/siRND3#2), *P = 0.0290 (mCit-RND3/siNT vs. mCit-RND3/siRND3(pool)).

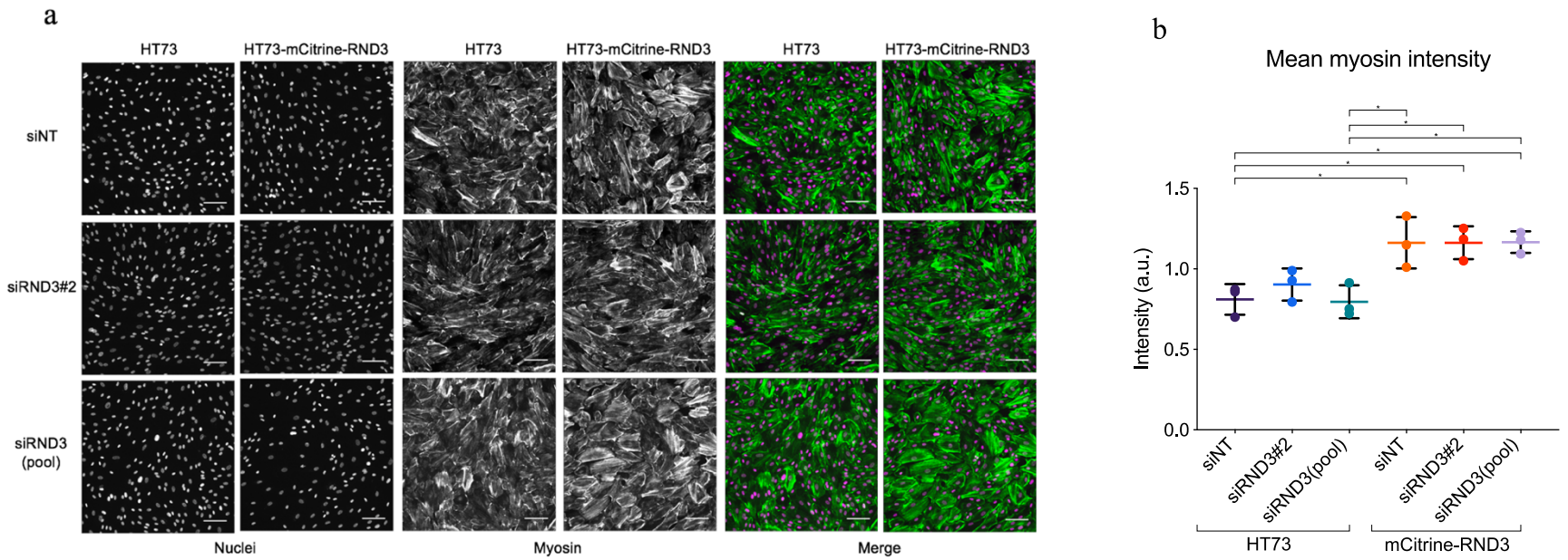

Figure 22. Effect of RND3 depletion and overexpression on the myosin cytoskeleton in parental HUVEC (HT73) and HUVEC containing the mCitrine-RND3 construct (HT73-mCitrine-RND3). Each data point represents a biological replicate (n = 3). **(a)** Immunofluorescence images of activated myosin-II, labelled with pMLC primary antibody and Alexa 647 goat anti-rabbit secondary antibody. Scale bars for all images are 100 μm. **(b)** Quantification of the mean fluorescence intensity of myosin measured in cytoplasmic rings surrounding the cell nuclei. Myosin fluorescence intensities were normalized and an ordinary one-way ANOVA and Tukey's multiple comparisons test was performed. *P = 0.0170 (HT73/siNT vs. mCit-RND3/siNT), *P = 0.0170 (HT73/siNT vs. mCit-RND3/siRND3#2), *P = 0.0158 (HT73/siNT vs. mCit-RND3/siRND3(pool)), *P = 0.0129 (HT73/siRND3(pool) vs. mCit-RND3/siNT), *P = 0.0129 (HT73/siRND3(pool) vs. mCit-RND3/siRND3#2), *P = 0.0120 (HT73/siRND3(pool) vs. mCit-RND3/siRND3(pool)).

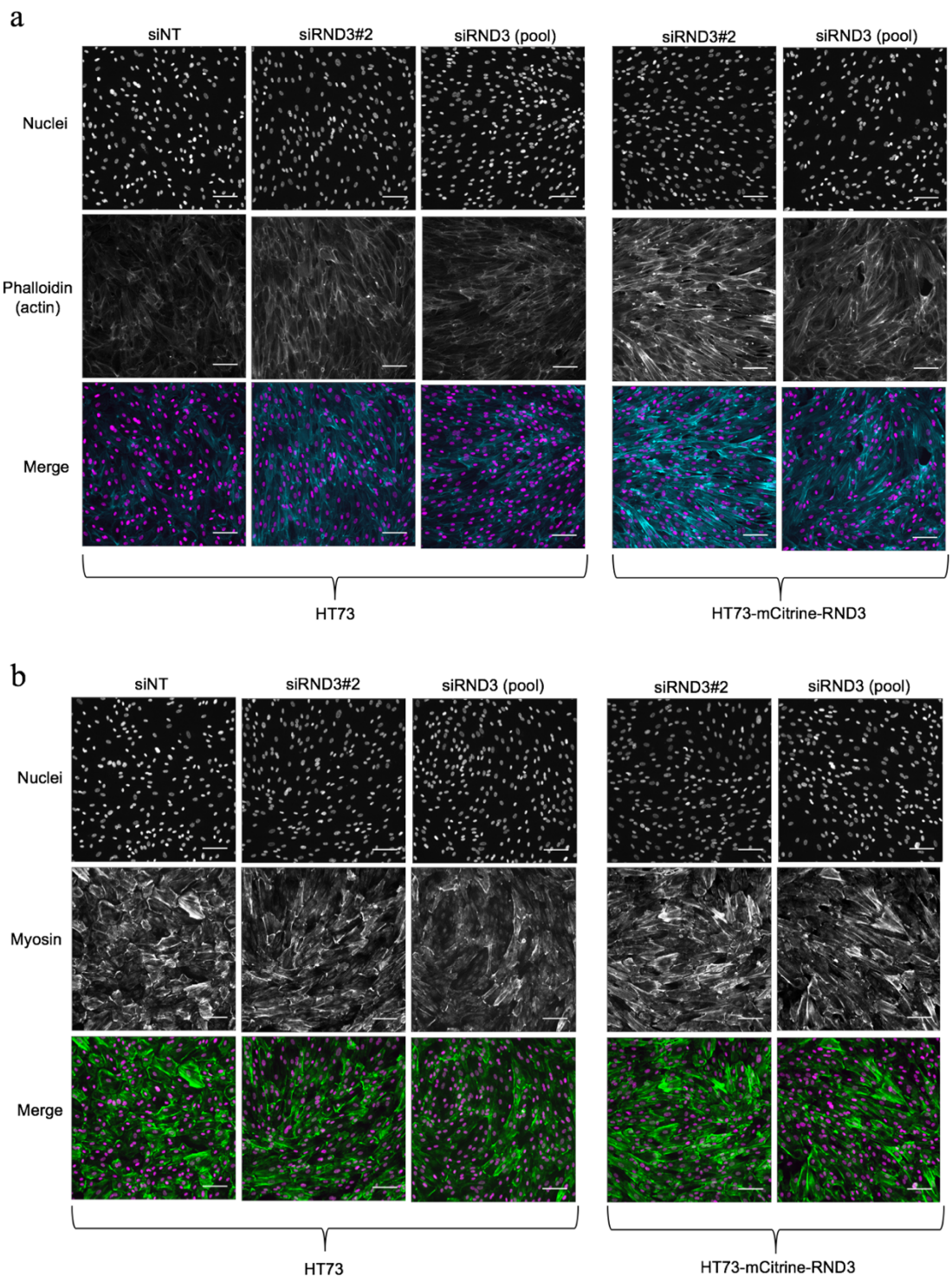

Figure 23. siRND3-treated cells are more elongated and organized in streams in both parental HUVEC (HT73) and in HUVEC containing the mCitrine-RND3 construct (HT73-mCitrine-RND3). **(a)** Immunofluorescence images of F-actin, labelled with phalloidin 555. **(b)** Immunofluorescence images of activated myosin-II, labelled with pMLC primary antibody and Alexa 647 goat anti-rabbit secondary antibody. Scale bars for all images are 100 μm.

4. DISCUSSION

The goal of this project was to learn more about the mechanisms regulating collective cell migration by focusing on two candidate regulators, FARP1 and RND3, identified from a previously performed siRNA screen. Using siRNA pool deconvolution, we attempted to validate the results obtained from a previously performed siRNA screen that knocked down expression of genes coding for Rho GEFs and Rho GTPases. This previous screen identified FARP1 and RND3 as candidate regulators of collective cell migration, where FARP1 knockdown decreased both velocity and coordination, and RND3 knockdown decreased velocity, but increased coordination. From the pool of 4 siRNAs, siFARP1#3 and siRND3#2 were found to reproduce the cell migration phenotypes previously observed. siRND3(pool) also showed an increase in coordination (however statistically not significant), although its reduction in velocity was not as low as with siRND3#2.

We further validated RND3 and FARP1 as candidate regulators by determining knockdown efficiency of the individual siRNAs using RT-qPCR. Since siFARP1#3 in the validation assay showed the strongest migration phenotype, we expected a correlated reduction in FARP1 mRNA levels. Although there was a decrease in the mRNA level of FARP1 using siFARP1#3, it was not lowered as much as compared with the other siRNAs such as siFARP1#1, siFARP1#4, and siFARP1(pool). In addition to this, siFARP1#2 did not knock down FARP1 mRNA at all. The fact that siFARP1#3 did not cause a knockdown as strong as #1, #4, or the pool suggested a lack of specificity of siFARP1#3 towards FARP1. siRNAs are known to have off-target effects that can be sequence dependent or independent, the former consisting of the degradation of the wrong mRNA due to sequence similarity between the siRNA sequence and an unrelated mRNA, and the latter originating from inadvertent interactions that are not well understood (Echeverri and Perrimon, 2006; Sharma and Rao, 2009). Using siRNA pools is one

way to mitigate this while increasing knockdown efficiency (Echeverri and Perrimon, 2006), however it does not guarantee that there will be no off-target effects. Although the phenotype observed matches the one from the original screen, the genotype does not reflect this, suggesting that these results could have been a false positive due to off-target effects. To verify and minimize this problem, there are siRNA selection tools that can identify possible off-targets of any specific siRNA, and can help one select an optimal siRNA with barely any off-target effects (Das et al., 2013). This may be something to look into and consider for the FARP1 siRNAs, since overall knockdown efficiency was weaker compared to RND3.

Studies have also shown that when verifying siRNA knockdown efficiency via RT-qPCR, results may be improved when using primers that localize to specific regions relative to the siRNA sequence, possibly reducing false negative results (Holmes et al., 2010; Shepard et al., 2005). It is also important to keep in mind that this is not seen with all genes and some primers are not as efficient at measuring mRNA knockdown by siRNA (Holmes et al., 2010). Primer sets used for FARP1 were either taken from the Harvard primer bank or from literature that also performed RT-qPCR on this gene. Therefore, they were not positioned relative to each of our specific siRNAs, which could explain why FARP1 knockdown with siFARP1#3 was not as strong and siFARP1#2 did not induce knockdown. To mitigate this issue, we can also use Western blotting to verify knockdown efficiency, provided reliable antibodies are available.

In addition, we were also unsuccessful in PCR-amplifying FARP1 from a cDNA library, which would have been required to create an siRNA-resistant rescue construct. FARP1 had three transcript variants/isoforms (NCBI). We selected the isoform that did not have any internal variance, and that was not different at the N- and C-termini. It is therefore unlikely that this isoform

was the reason for unsuccessful amplification of FARP1. For these reasons, we decided to stop working on FARP1 and instead focus only on RND3.

One of the most effective ways to ensure knockdown specificity and to rule out off-target effects is through phenotypic rescue, whereby a knockdown-resistant version of the gene is reintroduced into cells (Echeverri and Perrimon, 2006; Sharma and Rao, 2009). To confirm knockdown specificity, we selected siRND3#2 to create an siRNA-resistant rescue construct by generating synonymous mutations in the area where this particular siRNA binds. We also included an mCitrine tag to visualize RND3. For this rescue assay, we performed the same siRNA assay as the validation experiments mentioned above, except we now had two cell lines; the parental HUVEC (HT73) and HUVEC with the rescue construct (HT73-mCitrine-RND3), transfected with siRND3#2 and siRND3(pool). We considered the migration phenotype rescued if it partly or fully reverted back to control-treated cells, i.e. HT73 cells transfected with siNT. Compared to the siRNA validation assay, the cell density was slightly lower. We had some difficulty maintaining consistent densities throughout both cell lines because HT73-mCitrine-RND3 cells were larger and did not divide as quickly as HT73 cells, and this is shown in the cell density plot, where the density was higher for HT73 cells than for HT73-mCitrine-RND3 cells (**Figure 20a**). In the rescue assay, the trend and the values for velocity in HT73 cells transfected with siNT, siRND3#2, and siRND3(pool) was consistent with that seen in the validation assay. For coordination in the rescue assay (**Figure 20b**), the values for these same cells (HT73) transfected with these same siRNAs (siNT, siRND3#2, and siRND3(pool)) were lower than those in the validation assay (**Figure 17b**). This was unlikely due to cell density, because cell densities for HT73 cells were similar in both assays. The only difference between these two assays was that the validation experiments were done on 96-well plastic bottom plates, whereas the rescue experiments were done on 96-well glass

bottom plates. Although both were coated with collagen (plastic for 30 minutes the same day as the experiment, and glass for 24 hours), research has shown that the surface properties of collagen are dependent on the underlying substrate being coated (Harnett et al., 2007). A hydrophobic surface is generated when collagen is coated on plastic, whereas the surface becomes hydrophilic when collagen is coated on glass (Harnett et al., 2007). These differences could affect cell motility and could explain why coordination values in parental HUVEC in the validation experiments versus in the rescue experiments were quantitatively different. Our attempts to rescue the migration defects due to RND3 knockdown by expressing mCitrine-RND3 were not successful. Fusions of a fluorescent protein tag to a protein of interest can sometimes interfere with its function, especially when overexpressed (Crivat and Taraska, 2012). RND3 is a small atypical Rho GTPase of approximately 26 kDa (atlasgeneticsoncology.org) whereas mCitrine is roughly the same size at 27 kDa (Fluorescent protein database). Based on literature that fused GFP to the N-terminus of RND3 (Roberts et al., 2008), and because C-terminal fusion would have interfered with lipid modifications of the CAAX sequence, we fused mCitrine to RND3's N-terminus.

Nevertheless, with a tag as big as the protein itself, it cannot be excluded that the fluorescent tag interferes with RND3 function or folding and this may explain its inability to rescue the migration phenotype induced by siRND3#2. To address this, we have remade a similar siRNA-resistant rescue construct, but without the mCitrine tag, and plan to redo these experiments to see if a rescue actually occurs. Given the current data, we cannot yet exclude that the migration phenotype produced by siRND3#2 is due to off-target effects. We also do not believe that a specific RND3 isoform could be the reason that there was no phenotypic rescue. There are only two RND3 transcript variants, and both encode the same protein (NCBI). We selected the variant that was longer and that did not differ in the 5'UTR. Similarly to FARP1, RND3 did not differ at the N-

and C-termini and there was no internal variance. Another important aspect to consider is the expression level of the rescue construct. If RND3 overexpression is much higher than endogenous levels of RND3, then the rescue may possibly be affected by this, or result in misleading phenotypes. This highlights the importance of being able to visualize and quantify both exogenous and endogenous RND3. In our cells expressing untagged RND3, we will assess expression levels using antibodies against RND3.

We next investigated possible qualitative and quantitative changes in actin organization and myosin activity in cells overexpressing or depleted of RND3. We found that RND3 knockdown and RND3 overexpression both led to an increase in F-actin content, as assessed by phalloidin staining. At first, this result was unexpected. Multiple studies have shown that RND3 overexpression disrupts actin stress fibres (Guasch et al., 1998; Nobes et al., 1998; Riento et al., 2003, 2005; Wennerberg et al., 2003). The proposed mechanism by which this happens is that RND3 activates p190RhoGAP, which decreases RhoA activity and its target ROCK, inhibiting stress fibre formation (Priya et al., 2015; Wennerberg et al., 2003). However, these studies were done in non-endothelial cells. In HUVEC, the opposite effect can be seen; RND3, when expressed for longer periods of time causes an increase in stress fibres through an increase in RhoB expression (Gottesbühren et al., 2013). This increase in stress fibres occurred also when RND3 localized to the cytoplasm due to mutations: one mutant was unable to be posttranslationally modified, and the other mutant had its last few amino acids missing (Gottesbühren et al., 2013). RhoB is known to be regulated at the transcriptional and protein levels, but how RND3 is involved in this regulation is currently unknown (Gottesbühren et al., 2013).

The fact that an increase in actin is seen in RND3-depleted cells as well as in cells in which RND3 was overexpressed suggests two possible pathways that converge to affect actin stress

fibres/F-actin (**Figure 24**). When RND3 is knocked down, the suppression of Rho/ROCK by p190RhoGAP is relieved, causing an increase in stress fibres (similar to inhibiting and inhibitor). As previously mentioned, when RND3 is overexpressed, RhoB activity is increased, which activates ROCK and induces an increase in stress fibres/F-actin. However, if overexpression causes more RND3 to be present, it may also activate more p190RhoGAP leading to the suppression of Rho/ROCK and a reduction in stress fibres. The fact that overexpression causes stress fibre increase suggests that perhaps the overexpression effect may be stronger than the potentially increased suppression of the pathway involving p190RhoGAP. To test this, one could use RT-qPCR to measure the increase in RhoB expression, and to knock down RhoB at the same time that RND3 is overexpressed.

Previous studies have not focused on the way myosin activity specifically is affected by RND3 depletion or overexpression. However, we expected a change in myosin activity, detectable by increased pMLC immunofluorescence signal, particularly because myosin-II interacts with actin to form stress fibres and induces cell contraction when activated by Rho (Smith et al., 2010; Svitkina, 2018). Based on this, we hypothesized that if there were a change in F-actin/stress fibres, there would be a change in myosin activity as well, since RND3 affects Rho and downstream effectors. Consistent with this and as was seen for F-actin, RND3 overexpression resulted in an increase in myosin activity (pMLC signal), (**Figure 22**).

We also noticed striking morphological changes in siRND3-treated cells. Cells were more elongated and arranged in streams compared to cells treated with siNT (**Figure 23**). Although this has not yet been quantified, a change in cell morphology and organization is not unexpected, since RND3 affects actin and myosin structures. Future studies should address whether the effects of

RND3 knockdown on cell shape and alignment of cells within the monolayer are due to cell-intrinsic or cell non-autonomous effects.

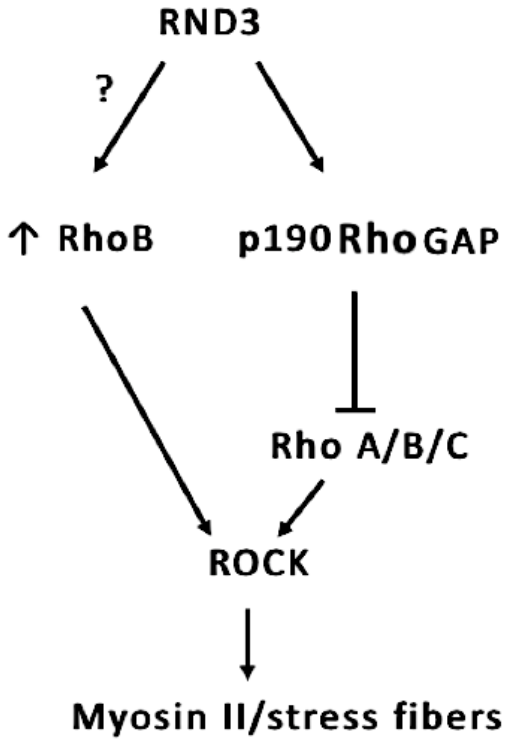

Figure 24. Possible mechanisms by which RND3 induces an increase in actin stress fibres.

5. CONCLUSION

The spatial and temporal regulation of Rho GTPase signalling is central in controlling cell migration, however the mechanisms by which such regulation is achieved are not yet fully understood. The work presented in this thesis provides new evidence in support for the atypical Rho GTPase RND3 being an important regulator of actin cytoskeletal dynamics during collective endothelial cell migration. Future experiments should aim to determine whether RND3 primarily regulates autonomous cell migration or whether it is involved in regulating coordination between cells across adhesive cell-cell contacts. One possible experimental approach to determine this is to study individual cells migrating along linear patterns of extracellular matrix. If movement of cells along such patterns is unaffected by RND3 depletion, then this argues that RND3 is involved in a cell-cell coupling mechanism that is important for collective cell migration. Whether RND3 acts through cell-cell junctions has yet to be determined. However, RND3 overexpression in endothelial cells was shown to induce an increase in actin stress fibres, corresponding to the disruption of the linear localization of VE-cadherin (Gottesbühren et al., 2013). Disrupting VE-cadherin-mediated cell-cell adhesion, either by using siRNAs targeting α-catenin, or by overexpressing a truncated version of VE-cadherin (Hayer et al., 2016), and simultaneously depleting RND3 from cells could be a suitable experimental approach to further uncouple the possible cell-autonomous and cell non-autonomous roles of RND3. Our findings will not only deepen our understanding of cell migration, but will also provide valuable insight into disease states where it is impaired.

6. REFERENCES

Amado-Azevedo, J., Reinhard, N.R., Van Bezu, J., De Menezes, R.X., Van Beusechem, V.W., Van Nieuw Amerongen, G.P., Van Hinsbergh, V.W.M., and Hordijk, P.L. (2017). A CDC42-centered signaling unit is a dominant positive regulator of endothelial integrity. Sci. Rep. *7*, 1–13.

Aspenström, P. (2018). Fast-cycling Rho GTPases. Small GTPases 1–8.

Aspenström, P., Ruusala, A., and Pacholsky, D. (2007). Taking Rho GTPases to the next level: The cellular functions of atypical Rho GTPases. Exp. Cell Res. *313*, 3673–3679.

Athey, J., Alexaki, A., Osipova, E., Rostovtsev, A., Santana-Quintero, L. V., Katneni, U., Simonyan, V., and Kimchi-Sarfaty, C. (2017). A new and updated resource for codon usage tables. BMC Bioinformatics *18*, 1–10.

Bagci, H., Sriskandarajah, N., Robert, A., Boulais, J., Elkholi, I.E., Tran, V., Lin, Z.Y., Thibault, M.P., Dubé, N., Faubert, D., et al. (2020). Mapping the proximity interaction network of the Rho-family GTPases reveals signalling pathways and regulatory mechanisms. Nat. Cell Biol. *22*, 120–134.

Bazzoni, G., and Dejana, E. (2004). Endothelial Cell-to-Cell Junctions: Molecular Organization and Role in Vascular Homeostasis. Physiol. Rev. *84*, 869–901.

Bektic, J., Pfeil, K., Berger, A.P., Ramoner, R., Pelzer, A., Schäfer, G., Kofler, K., Bartsch, G., and Klocker, H. (2005). Small G-protein RhoE is Underexpressed in Prostate Cancer and Induces Cell Cycle Arrest and Apoptosis. Prostate *64*, 332–340.

Bernard, O. (2007). Lim kinases, regulators of actin dynamics. Int. J. Biochem. Cell Biol. *39*, 1071–1076.

Bolós, V., Gasent, J.M., López-Tarruella, S., and Grande, E. (2010). The dual kinase complex FAK-Src as a promising therapeutic target in cancer. Onco. Targets. Ther. *3*, 83–97.

Bos, J., Rehmann, H., and Wittinghofer, A. (2007). GEFs and GAPs : Critical Elements in the Control of Small G Proteins. Cell *129*, 865–877.

Van Buul, J.D., Geerts, D., and Huveneers, S. (2014). Rho GAPs and GEFs: Controling switches in endothelial cell adhesion. Cell Adhes. Migr. *8*, 108–124.

Cerutti, C., and Ridley, A.J. (2017). Endothelial cell-cell adhesion and signaling. Exp. Cell Res. *358*, 31–38.

Chardin, P. (2006). Function and regulation of Rnd proteins. Nat. Rev. Mol. Cell Biol. *7*, 54–62.

Cheadle, L., and Biederer, T. (2012). The novel synaptogenic protein Farp1 links postsynaptic cytoskeletal dynamics and transsynaptic organization. J. Cell Biol. *199*, 985–1001.

Cherfils, J., and Zeghouf, M. (2013). Regulation of Small GTPases by GEFs, GAPs, and GDIs. Physiol. Rev. *93*, 269–309.

Cook, D.R., Rossman, K.L., and Der, C.J. (2014). Rho guanine nucleotide exchange factors: regulators of Rho GTPase activity in development and disease. Oncogene *33*, 4021–4035.

Crivat, G., and Taraska, J.W. (2012). Imaging proteins inside cells with fluorescent tags. Trends Biotechnol. *30*, 8–16.

Croisé, P., Houy, S., Gand, M., Lanoix, J., Calco, V., Tóth, P., Brunaud, L., Lomazzi, S., Paramithiotis, E., Chelsky, D., et al. (2016). Cdc42 and Rac1 activity is reduced in human pheochromocytoma and correlates with FARP1 and ARHGEF1 expression. Endocr. Relat. Cancer *23*, 281–293.

Croisé, P., Brunaud, L., Tóth, P., Gasman, S., and Ory, S. (2017). Inhibition of Cdc42 and Rac1 activities in pheochromocytoma, the adrenal medulla tumor. Small GTPases *8*, 122–127.

Das, S., Ghosal, S., Kozak, K., and Chakrabarti, J. (2013). An siRNA designing tool with a unique functional off-target filtering approach. J. Biomol. Struct. Dyn. *31*, 1343–1357.

Dejana, E. (2004). Endothelial cell-cell junctions: Happy together. Nat. Rev. Mol. Cell Biol. *5*, 261–270.

Dejana, E., Corada, M., and Lampugnani, M.G. (1995). Endothelia cell-to-cell junctions. FASEB *9*, 910–918.

Devreotes, P., and Horwitz, A.R. (2015). Signaling Networks that Regulate Cell Migration. Cold Spring Harb. Perspect. Biol. *7*, a005959.

Dorland, Y.L., and Huveneers, S. (2016). Cell–cell junctional mechanotransduction in endothelial remodeling. Cell. Mol. Life Sci. *74*, 279–292.

Ebnet, K., Kummer, D., Steinbacher, T., Singh, A., Nakayama, M., and Matis, M. (2018). Regulation of cell polarity by cell adhesion receptors. Semin. Cell Dev. Biol. *81*, 2–12.

Echeverri, C.J., and Perrimon, N. (2006). High-throughput RNAi screening in cultured cells: a user's guide. Nat. Rev. Genet. *7*, 373–384.

Farooqui, R., and Fenteany, G. (2005). Multiple rows of cells behind an epithelial wound edge extend cryptic lamellipodia to collectively drive cell-sheet movement. J. Cell Sci. *118*, 51–63.

Feng, B., Li, K., Zhong, H., Ren, G., Wang, H., Shang, Y., Bai, M., Liang, J., Wang, X., and Fan, D. (2013). RhoE Promotes Metastasis in Gastric Cancer through a Mechanism Dependent on Enhanced Expression of CXCR4. PLoS One *8*, e81709.

Foster, R., Hu, K.Q., Lu, Y., Nolan, K.M., Thissen, J., and Settleman, J. (1996). Identification of a Novel Human Rho Protein with Unusual Properties: GTPase Deficiency and In Vivo Farnesylation. Mol. Cell. Biol. *16*, 2689–2699.

Friedl, P., and Mayor, R. (2017). Tuning Collective Cell Migration by Cell-Cell Junction Regulation. Cold Spring Harb. Perspect. Biol. *9*, a029199.

Fritz, R.D., and Pertz, O. (2016). The dynamics of spatio-temporal Rho GTPase signaling: formation of signaling patterns. F1000Research *5*, 1–12.

García-Mata, R., and Burridge, K. (2007). Catching a GEF by its tail. Trends Cell Biol. *17*, 36–43.

Goicoechea, S.M., Awadia, S., and Garcia-Mata, R. (2014). I'm coming to GEF you: Regulation of RhoGEFs during cell migration. Cell Adhes. Migr. *8*, 535–549.

Gottesbühren, U., Garg, R., Riou, P., McColl, B., Brayson, D., and Ridley, A.J. (2013). Rnd3 induces stress fibres in endothelial cells through RhoB. Biol. Open *2*, 210–216.

Guasch, R.M., Scambler, P., Jones, G.E., and Ridley, A.J. (1998). RhoE Regulates Actin Cytoskeleton Organization and Cell Migration. Mol. Cell. Biol. *18*, 4761–4771.

Hanna, S., and El-Sibai, M. (2013). Signaling networks of Rho GTPases in cell motility. Cell. Signal. *25*, 1955–1961.

Hannus, M., Beitzinger, M., Engelmann, J.C., Weickert, M.T., Spang, R., Hannus, S., and Meister, G. (2014). siPools: highly complex but accurately defined siRNA pools eliminate off-target effects. Nucleic Acids Res. *42*, 8049–8061.

Harnett, E.M., Alderman, J., and Wood, T. (2007). The surface energy of various biomaterials coated with adhesion molecules used in cell culture. Colloids Surfaces B Biointerfaces *55*, 90–97.

Hayer, A., Shao, L., Chung, M., Joubert, L.M., Yang, H.W., Tsai, F.C., Bisaria, A., Betzig, E., and Meyer, T. (2016). Engulfed cadherin fingers are polarized junctional structures between collectively migrating endothelial cells. Nat. Cell Biol. *18*, 1311–1323.

He, X., Kuo, Y.C., Rosche, T.J., and Zhang, X. (2013). Structural Basis for Autoinhibition of the Guanine Nucleotide Exchange Factor FARP2. Structure *21*, 355–364.

Hirano, T., Shinsato, Y., Tanabe, K., Higa, N., Kamil, M., Kawahara, K., Yamamoto, M., Minami, K., Shimokawa, M., Arigami, T., et al. (2020). FARP1 boosts CDC42 activity from integrin αvβ5 signaling and correlates with poor prognosis of advanced gastric cancer. Oncogenesis *9*, 1–14.

Hodge, R.G., and Ridley, A.J. (2016). Regulating Rho GTPases and their regulators. Nat. Rev. Mol. Cell Biol. *17*, 496–510.

Holmes, K., Williams, C.M., Chapman, E.A., and Cross, M.J. (2010). Detection of siRNA induced mRNA silencing by RT-qPCR: considerations for experimental design. BMC Res. Notes *3*, 1–5.

Horwitz, R., and Webb, D. (2003). Cell migration. Curr. Biol. *13*, R756-759.

Huttenlocher, A., Sandborg, R.R., and Horwitz, A.F. (1995). Adhesion in cell migration. Curr. Opin. Cell Biol. *7*, 697–706.

Ilina, O., and Friedl, P. (2009). Mechanisms of collective cell migration at a glance. J. Cell Sci. *122*, 3203–3208.

Jie, W., Andrade, K.C., Lin, X., Yang, X., Yue, X., and Chang, J. (2016). Pathophysiological Functions of Rnd3/RhoE. Compr. Physiol. *6*, 169–186.

Klein, R.M., and Aplin, A.E. (2009). Rnd3 Regulation of the Actin Cytoskeleton Promotes Melanoma Migration and Invasive Outgrowth in 3-D. Cancer Res. *69*, 2224–2233.

Kuo, Y.-C., He, X., Coleman, A.J., Chen, Y.-J., Dasari, P., Liou, J., Biederer, T., and Zhang, X. (2018). Structural analyses of FERM domain-mediated membrane localization of FARP1. Sci. Rep. *8*, 10477.

Lawson, C.D., and Burridge, K. (2014). The on-off relationship of Rho and Rac during integrin-mediated adhesion and cell migration. Small GTPases *5*, e27958.

Livak, K.J., and Schmittgen, T.D. (2001). Analysis of Relative Gene Expression Data Using Real-Time Quantitative PCR and the 2-ΔΔCT Method. Methods *25*, 402–408.

Llense, F., and Etienne-Manneville, S. (2015). Front-to-Rear Polarity in Migrating Cells. In Cell Polarity 1: Biological Role and Basic Mechanisms, pp. 115–146.

Mayor, R., and Carmona-Fontaine, C. (2010). Keeping in touch with contact inhibition of locomotion. Trends Cell Biol. *20*, 319–328.

Mayor, R., and Etienne-Manneville, S. (2016). The front and rear of collective cell migration. Nat. Rev. Mol. Cell Biol. *17*, 97–109.

Müller, P.M., Rademacher, J., Bagshaw, R.D., Wortmann, C., Barth, C., van Unen, J., Alp, K.M., Giudice, G., Eccles, R.L., Heinrich, L.E., et al. (2020). Systems analysis of RhoGEF and RhoGAP regulatory proteins reveals spatially organized RAC1 signalling from integrin adhesions. Nat. Cell Biol. *22*, 498–511.

Nobes, C.D., Lauritzen, I., Mattei, M.G., Paris, S., Hall, A., and Chardin, P. (1998). A New Member of the Rho Family, Rnd1, Promotes Disassembly of Actin Filament Structures and Loss of Cell Adhesion. J. Cell Biol. *141*, 187–197.

Ota, T., Maeda, M., Okamoto, M., and Tatsuka, M. (2015). Positive regulation of Rho GTPase activity by RhoGDIs as a result of their direct interaction with GAPs. BMC Syst. Biol. *9*, 1–9.

Paduch, M., Jeleń, F., and Otlewski, J. (2001). Structure of small G proteins and their regulators. Acta Biochim. Pol. *48*, 829–850.

Paysan, L., Piquet, L., Saltel, F., and Moreau, V. (2016). Rnd3 in Cancer: A Review of the Evidence for Tumor Promoter or Suppressor. Mol. Cancer Res. *14*, 1033–1044.

Priya, R., Gomez, G.A., Budnar, S., Verma, S., Cox, H.L., Hamilton, N.A., and Yap, A.S. (2015). Feedback regulation through myosin II confers robustness on RhoA signalling at E-cadherin junctions. Nat. Cell Biol. *17*, 1282–1293.

Prunier, C., Prudent, R., Kapur, R., Sadoul, K., and Lafanechère, L. (2017). LIM kinases: cofilin and beyond. Oncotarget *8*, 41749–41763.

Raftopoulou, M., and Hall, A. (2004). Cell migration: Rho GTPases lead the way. Dev. Biol. *265*, 23–32.

Rahimi, N. (2017). Defenders and Challengers of Endothelial Barrier Function. Front. Immunol. *8*, 1847.

Ridley, A.J. (2011). Life at the Leading Edge. Cell *145*, 1012–1022.

Ridley, A.J. (2015). Rho GTPase signalling in cell migration. Curr. Opin. Cell Biol. *36*, 103–112.

Ridley, A.J., Schwartz, M.A., Burridge, K., Firtel, R.A., Ginsberg, M.H., Borisy, G., Parsons, J.T., and Horwitz, A.R. (2003). Cell Migration: Integrating Signals from Front to Back. Science (80-.). *302*, 1704–1709.

Riento, K., Guasch, R.M., Garg, R., Jin, B., and Ridley, A.J. (2003). RhoE Binds to ROCK I and Inhibits Downstream Signaling. Mol. Cell. Biol. *23*, 4219–4229.

Riento, K., Totty, N., Villalonga, P., Garg, R., Guasch, R., and Ridley, A.J. (2005). RhoE function is regulated by ROCK I-mediated phosphorylation. EMBO J. *24*, 1170–1180.

Riou, P., Kjær, S., Garg, R., Purkiss, A., George, R., Cain, R.J., Bineva, G., Reymond, N., McColl, B., Thompson, A.J., et al. (2013). 14-3-3 Proteins Interact with a Hybrid Prenyl-Phosphorylation Motif to Inhibit G Proteins. Cell *153*, 640–653.

Roberts, P.J., Mitin, N., Keller, P.J., Chenette, E.J., Madigan, J.P., Currin, R.O., Cox, A.D., Wilson, O., Kirschmeier, P., and Der, C.J. (2008). Rho Family GTPase Modification and Dependence on CAAX Motif-Signaled Posttranslational Modification. J. Biol. Chem. *283*, 25150–25163.

Rørth, P. (2009). Collective Cell Migration. Annu. Rev. Cell Dev. Biol. *25*, 407–429.

Scarpa, E., and Mayor, R. (2016). Collective cell migration in development. J. Cell Biol. *212*, 143–155.

Schaefer, A., Reinhard, N.R., and Hordijk, P.L. (2014). Toward understanding RhoGTPase specificity: structure, function and local activation. Small GTPases *5*, 1–11.

Scheswohl, D.M., Harrell, J.R., Rajfur, Z., Gao, G., Campbell, S.L., and Schaller, M.D. (2008). Multiple paxillin binding sites regulate FAK function. J. Mol. Signal. *3*, 1–11.

Schmidt, A., and Hall, A. (2002). Guanine nucleotide exchange factors for Rho GTPases: Turning on the switch. Genes Dev. *16*, 1587–1609.

Schwaid, A.G., Su, C., Loos, P., Wu, J., Nguyen, C., Stone, K.L., Kanyo, J., Geoghegan, K.F., Bhattacharya, S.K., Dow, R.L., et al. (2015). MAP4K4 Is a Threonine Kinase That Phosphorylates FARP1. ACS Chem. Biol. *10*, 2667–2671.

Sharma, S., and Rao, A. (2009). RNAi screening: tips and techniques. Nat. Immunol. *10*, 799–804.

Shepard, A.R., Jacobson, N., and Clark, A.F. (2005). Importance of quantitative PCR primer location for short interfering RNA efficacy determination. Anal. Biochem. *344*, 287–288.

Smith, M.A., Blankman, E., Gardel, M.L., Luettjohann, L., Clare, M., and Beckerle, M.C. (2010). A Zyxin-Mediated Mechanism for Actin Stress Fiber Maintenance and Repair. *19*, 365–376.

Steinbacher, T., and Ebnet, K. (2018). The regulation of junctional actin dynamics by cell adhesion receptors. Histochem. Cell Biol. *150*, 341–350.

Svitkina, T. (2018). The Actin Cytoskeleton and Actin-Based Motility. Cold Spring Harb. Perspect. Biol. *10*, a018267.

Uhlén, M., Fagerberg, L., Hallström, B.M., Lindskog, C., Oksvold, P., Mardinoglu, A., Sivertsson, Å., Kampf, C., Sjöstedt, E., Asplund, A., et al. (2015). Tissue-based map of the human proteome. Science (80-.). *347*.

Vega, F.M., and Ridley, A.J. (2008). Rho GTPases in cancer cell biology. FEBS Lett. *582*, 2093–2101.

Vetter, I.R., and Wittinghofer, A. (2001). The Guanine Nucleotide-Binding Switch in Three Dimensions. Science (80-.). *294*, 1299–1304.

Virbasius, J. V., and Czech, M.P. (2016). Map4k4 Signaling Nodes in Metabolic and Cardiovascular Diseases. Trends Endocrinol. Metab. *27*, 484–492.

Vitorino, P., Yeung, S., Crow, A., Bakke, J., Smyczek, T., West, K., McNamara, E., Eastham-Anderson, J., Gould, S., Harris, S.F., et al. (2015). MAP4K4 regulates integrin-FERM binding to control endothelial cell motility. Nature *519*, 425–430.

Wennerberg, K., Forget, M.-A., Ellerbroek, S.M., Arthur, W.T., Burridge, K., Settleman, J., Der, C.J., and Hansen, S.H. (2003). Rnd Proteins Function as RhoA Antagonists by Activating p190 RhoGAP. Curr. Biol. *13*, 1106–1115.

Zegers, M.M., and Friedl, P. (2014). Rho GTPases in collective cell migration. Small GTPases *5*, e28997.

Zhu, Y., Zhou, J., Xia, H., Chen, X., Qiu, M., Huang, J., Liu, S., Tang, Q., Lang, N., Liu, Z., et al. (2014). The Rho GTPase RhoE is a p53-regulated candidate tumor suppressor in cancer cells. Int. J. Oncol. *44*, 896–904.